PR12-25-010, JLab PAC 53

Double Deeply Virtual Compton Scattering with SoLIDμ spectrometer

Juan-Sebastian Alvarado, IJCLab
Alexandre Camsonne, Jlab (contact)
Marie Boer, Virginia Tech
Eric Voutier, IJCLab
Xinzhan Bai, JLab
Zhiwen Zhao, Duke (presenter)

and SoLID Collaboration

July 21, 2025

Outline

- Generalized Parton Distribution
- Double Deeply Virtual Compton Scattering
- SoLIDμ setup
- Muon detector
- Simulation study
- Physics projection
- Beam time request
- Summary

Generalized Parton Distribution (GPD)

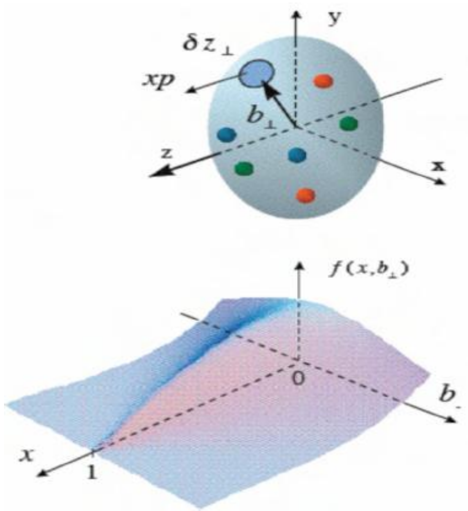

A unified description of partons (quarks and gluons) in the momentum and impact parameter space

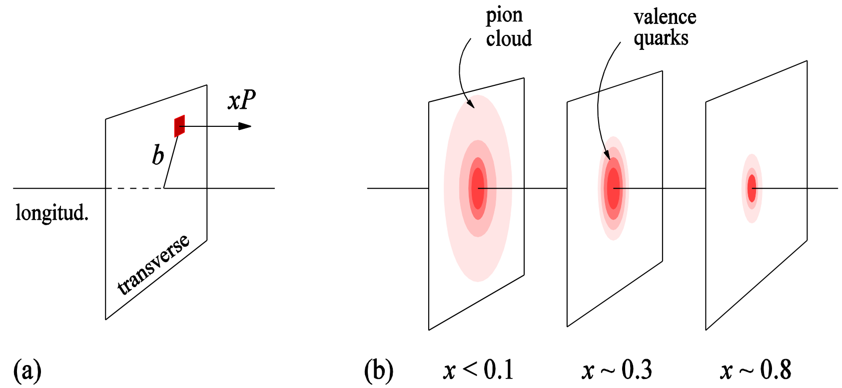

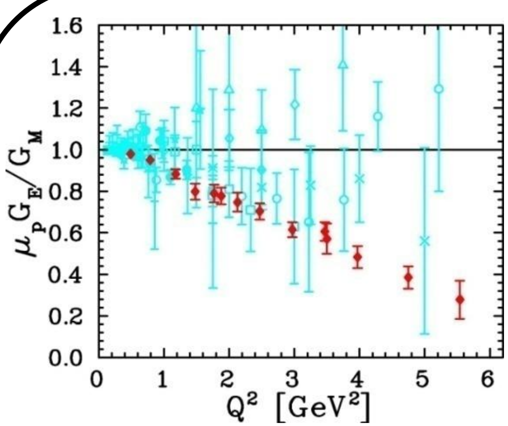

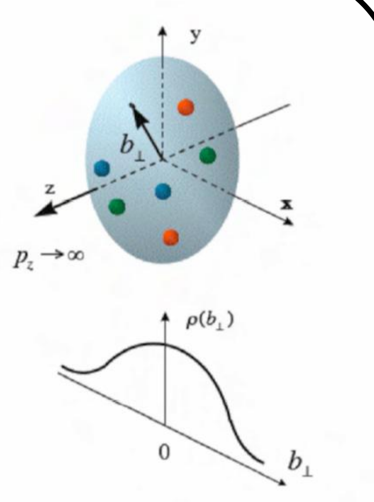

Elastic form factors

Transverse spatial distributions

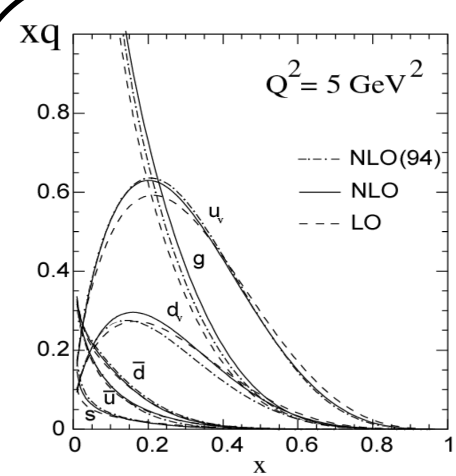

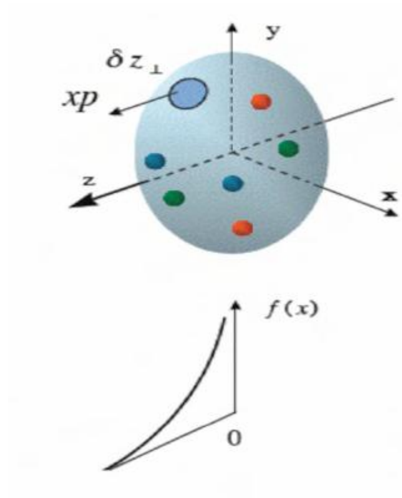

Parton Distribution Functions

Longitudinal momentum distributions

Nucleon Structure and GPD

GPDs encode **correlations between partons** and contain information about **internal dynamics of hadrons** like **angular momentum** or **distribution of the forces** experienced by quarks and gluons

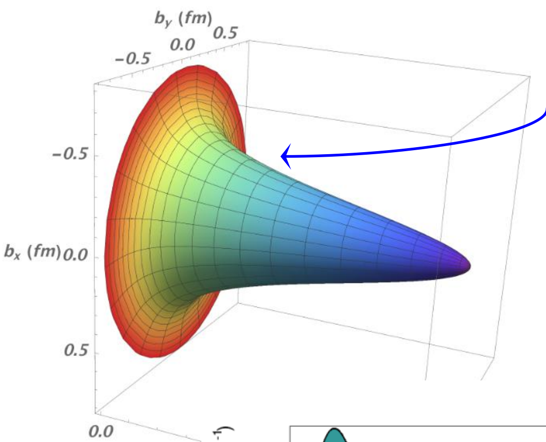

imaging

$$\rho_H^q(x,\boldsymbol{b}_\perp) = \int \frac{d^2\boldsymbol{\Delta}_\perp}{(2\pi)^2}\, e^{i\boldsymbol{b}_\perp\cdot\boldsymbol{\Delta}_\perp}\,[H^q(x,0,-\Delta_\perp^2) + H^q(-x,0,-\Delta_\perp^2)]$$

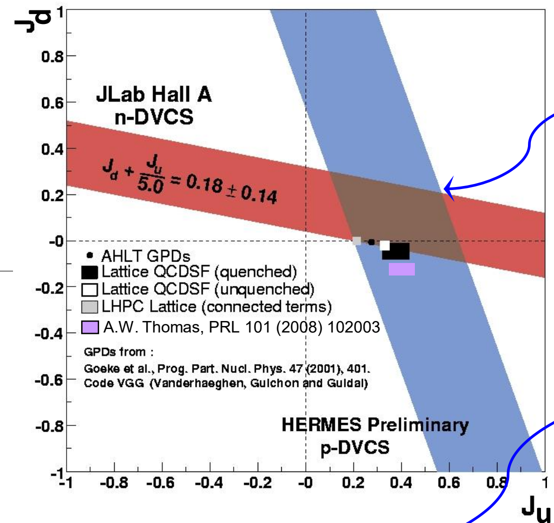

spin

$$\lim_{t\to 0}\int_{-1}^{1} x\,[H^q(x,\xi,t) + E^q(x,\xi,t)]\,dx = J^q$$

gravitational form factor

$$\int_{-1}^{1} x \sum_q H^q(x,\xi,t)\;dx = M_2(t) + \frac{4}{5}\xi^2 d_1(t)$$

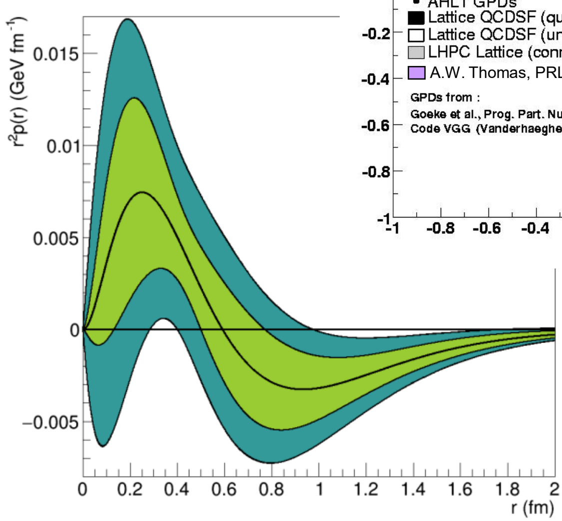

The **experimental knowledge** of the **ξ-dependence** of GPDs at fixed longitudinal momentum fraction is a **crucial step** for unraveling the 3D structure and internal dynamics of the **nucleon**

General Compton Process accessing GPD

$$\gamma^*(q) + p(p) \rightarrow \gamma^*(q') + p(p')$$

$$Q^2 = -q^2, \quad Q'^2 = q'^2, \quad s = (p+q)^2, \quad t = \Delta^2,$$

DVCS	**($\gamma^* \rightarrow \gamma$, Q'^2=0, $\xi' = \xi$)**
Timelike CS	**($\gamma \rightarrow \gamma^*$, Q^2=0, $\xi' = -\xi$)**
Double DVCS	**($\gamma^* \rightarrow \gamma^*$, Q^2 Q'^2 ξ' ξ vary)**

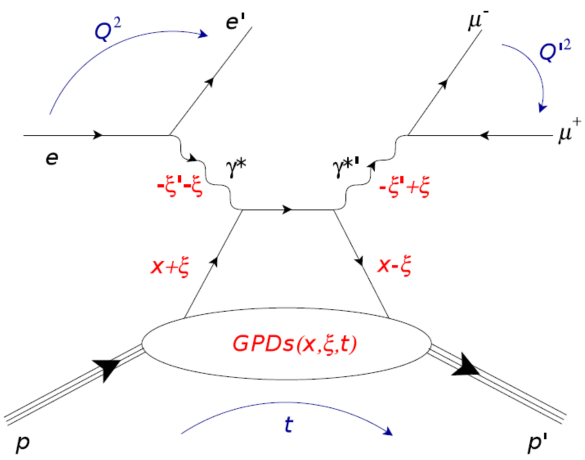

Because of the virtuality of the initial and final photon, **DDVCS** allows direct access to GPDs at $|x| < \xi$, crucial for modeling and investigation of **nuclear imaging, spin, and internal dynamics**

Compton Form Factor (CFF)

$$\mathcal{F}(\xi', \xi, t) = \mathcal{P} \int_{-1}^{1} F_+(x, \xi, t) \left[\frac{1}{x - \xi'} \pm \frac{1}{x + \xi'} \right] dx - i\pi F_+(\xi', \xi, t)$$

GPD combination

$$F_+(x, \xi, t) = \sum_q \left(\frac{e_q}{e} \right)^2 [F^q(x, \xi, t) \mp F^q(-x, \xi, t)]$$

Generalized Bjorken variable $\xi' = \dfrac{Q^2 - Q'^2 + t/2}{2Q^2/x_B - Q^2 - Q'^2 + t}$ Skewness $\xi = \dfrac{Q^2 + Q'^2}{2Q^2/x_B - Q^2 - Q'^2 + t}$

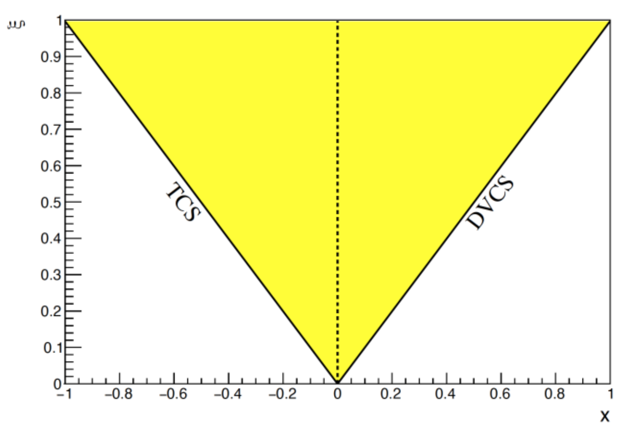

Following the sign change of ξ' around Q'^2=Q^2, the imaginary part of $\mathcal{H}$ and $\mathcal{E}$ **change sign**, providing a testing ground of **GPD universality**.

Elementary Cross Section

DDVCS cross section is about ~1/100 of DVCS, involves two Bethe-Heitler (BH) processes

$$d^7\sigma_P^e = d^7\sigma_{BH_1} + d^7\sigma_{BH_2} + d^7\sigma_{DDVCS} + P\, d^7\tilde{\sigma}_{DDVCS} + d^7\sigma_{INT_2} + P\, d^7\tilde{\sigma}_{INT_2} - e\left[d^7\sigma_{BH_{12}} + d^7\sigma_{INT_1} + P\, d^7\tilde{\sigma}_{INT_1}\right]$$

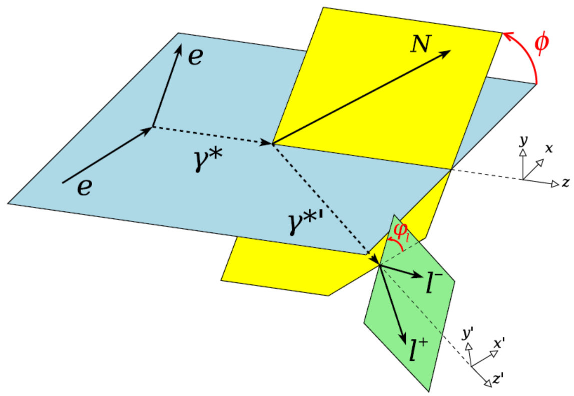

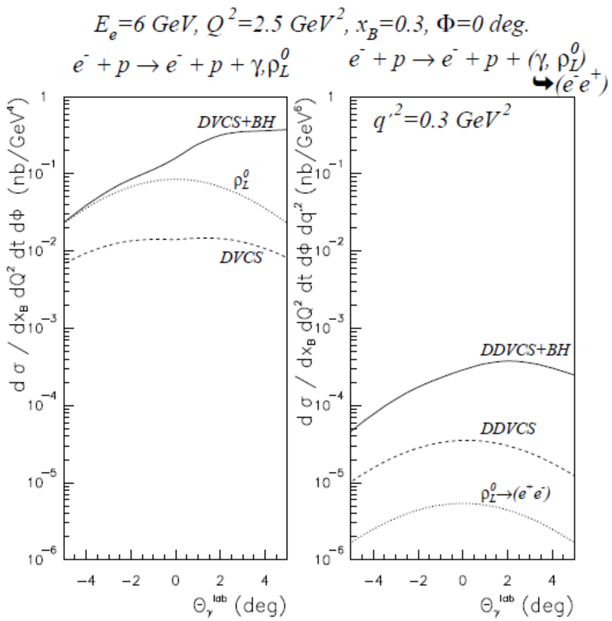

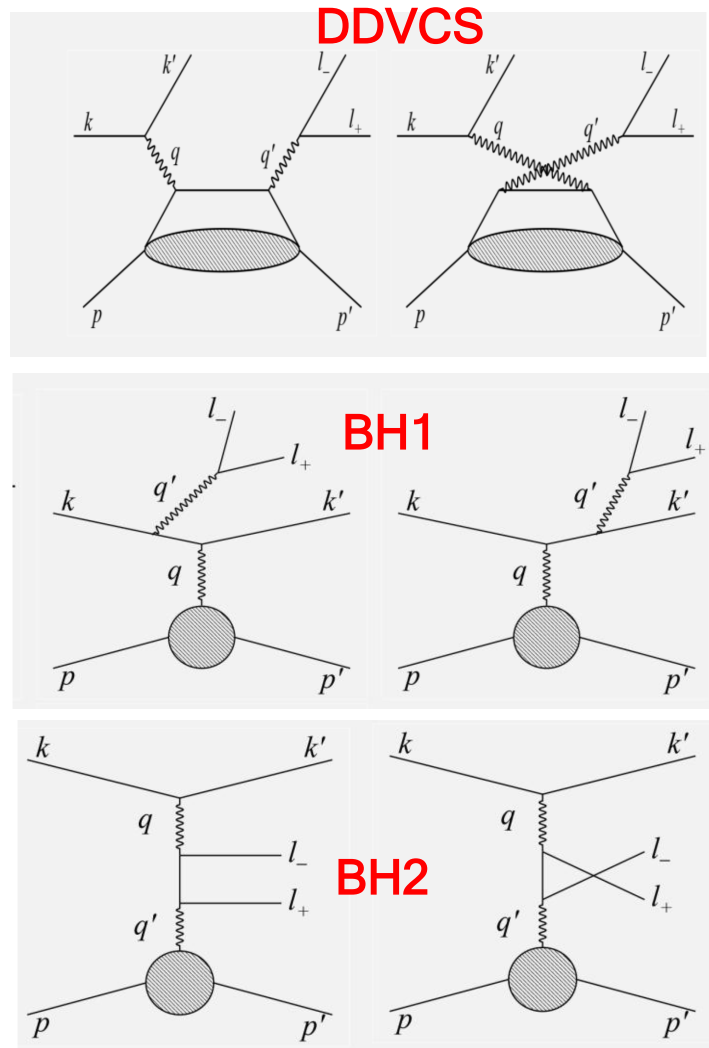

Integrated Cross Section

5-fold TCS-like observables obtained from the **integration** over the **polar angle** of **muon** and the **azimuthal angle** of **initial virtual photon**, also **minimizing** the contribution of the **BH_2** process

$\theta_0=\pi/4$

$$d^5\Sigma^\lambda(\varphi_\mu) \equiv \frac{d^5\sigma^\lambda(\varphi_\mu)}{dx_B\,dy\,dt\,dQ'^2\,d\varphi_\mu} = \int_0^{2\pi} d\phi \int_{\pi/2-\theta_0}^{\pi/2+\theta_0} d\theta_\mu \sin(\theta_\mu)\,\frac{d^7\sigma^\lambda(\phi,\theta_\mu,\phi_\mu)}{dx_B\,dy\,dt\,d\phi\,dQ'^2\,d\Omega_\mu}$$

$$d^5\Sigma^\lambda = d^5\Sigma_{BH_1} + d^5\Sigma_{BH_2} + d^5\Sigma_{BH_{12}} + d^5\Sigma_{DDVCS} + d^5\Sigma_{\mathcal{I}_1} + d^5\Sigma_{\mathcal{I}_2} + \lambda\, d^5\widetilde{\Sigma}_{\mathcal{I}_2} = d^5\Sigma_{UU} + \lambda\, d^5\Sigma_{LU}$$

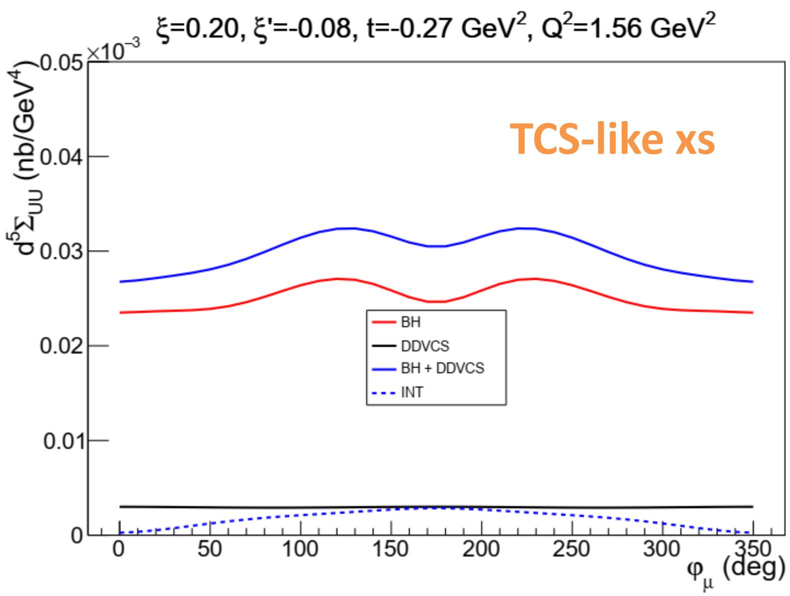

- Our study focuses on using **TCS-like observables** for projection to allow access to both terms above
- DVCS-like observables obtained by integrating over muon phi angle may also be considered as crosscheck

Beam Spin Asymmetry

$$A_{LU}^{\Sigma^\lambda}(\varphi_\mu) = \lambda \frac{d^5\Sigma^+ - d^5\Sigma^-}{d^5\Sigma^+ + d^5\Sigma^-} = \frac{\lambda\, d^5\widetilde{\Sigma}_{\mathcal{I}_2}}{d^5\Sigma_{BH_1} + d^5\Sigma_{BH_2} + d^5\Sigma_{BH_{12}} + d^5\Sigma_{DDVCS} + d^5\Sigma_{\mathcal{I}_1} + d^5\Sigma_{\mathcal{I}_2}}$$

$$\propto \Im\mathrm{m}\left\{F_1\mathcal{H} + \xi'(F_1+F_2)\widetilde{\mathcal{H}} - \frac{t}{4M_N^2}F_2\mathcal{E}\right\}$$

- Access to the imaginary part of CFFs
- **BSA** changes sign when transitioning from DVCS-like region ($\xi'>0$, $Q^2>Q'^2$) to TCS-like region ($\xi'<0$, $Q^2<Q'^2$)
- **DDVCS BSAs** are dominated by the CFF $\mathcal{H}$, thus providing a measurement of the $\mathcal{H}$ GPD at $\xi' \neq \pm\,\xi$ with similar quality to DVCS

BSA in two regions

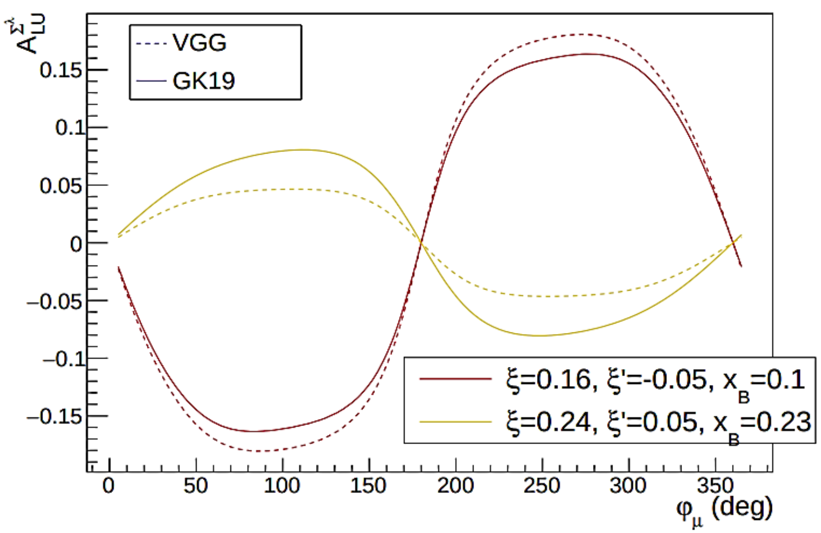

Muon Charge Asymmetry

$$A_{UU}^{\mu^\pm}(\varphi_\mu) = \frac{d^5\Sigma_{UU}(\varphi_{\mu^-}) - d^5\Sigma_{UU}(\varphi_{\mu^+})}{d^5\Sigma_{UU}(\varphi_{\mu^-}) + d^5\Sigma_{UU}(\varphi_{\mu^+})}$$

$$= \frac{d^5\Sigma_{BH_{12}} + d^5\Sigma_{\mathcal{I}_2}}{d^5\Sigma_{BH_1} + d^5\Sigma_{BH_2} + d^5\Sigma_{DDVCS} + d^5\Sigma_{\mathcal{I}_1}}$$

$$d^5\Sigma_{\mathcal{I}_2} \propto -\frac{\xi'}{\xi}\Re\mathfrak{e}\left[F_1\mathcal{H} + \frac{\xi^2}{\xi'}(F_1+F_2)\tilde{\mathcal{H}} - \frac{t}{4M_N^2}F_2\mathcal{E}\right]$$

aka Forward Backward Asymmetry

μCA in two regions

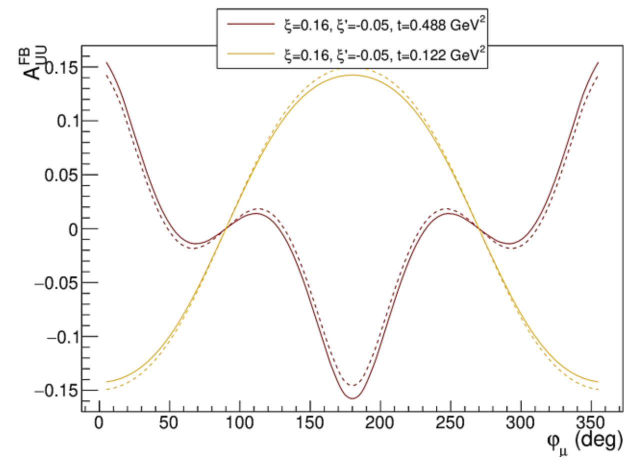

- Access to the real part of CFFs (no dispersion relation has been established)
- **μCA** predicted to have **significant amplitude** and rich **harmonic composition**, like the forward-backward asymmetry of TCS
- **Curvature change** is a highly-discriminating feature for models
- **DDVCS μCA** access a CFF combination **different** from **BSA**. This feature **distinguishes DDVCS** from DVCS and TCS.

Experimental Setup

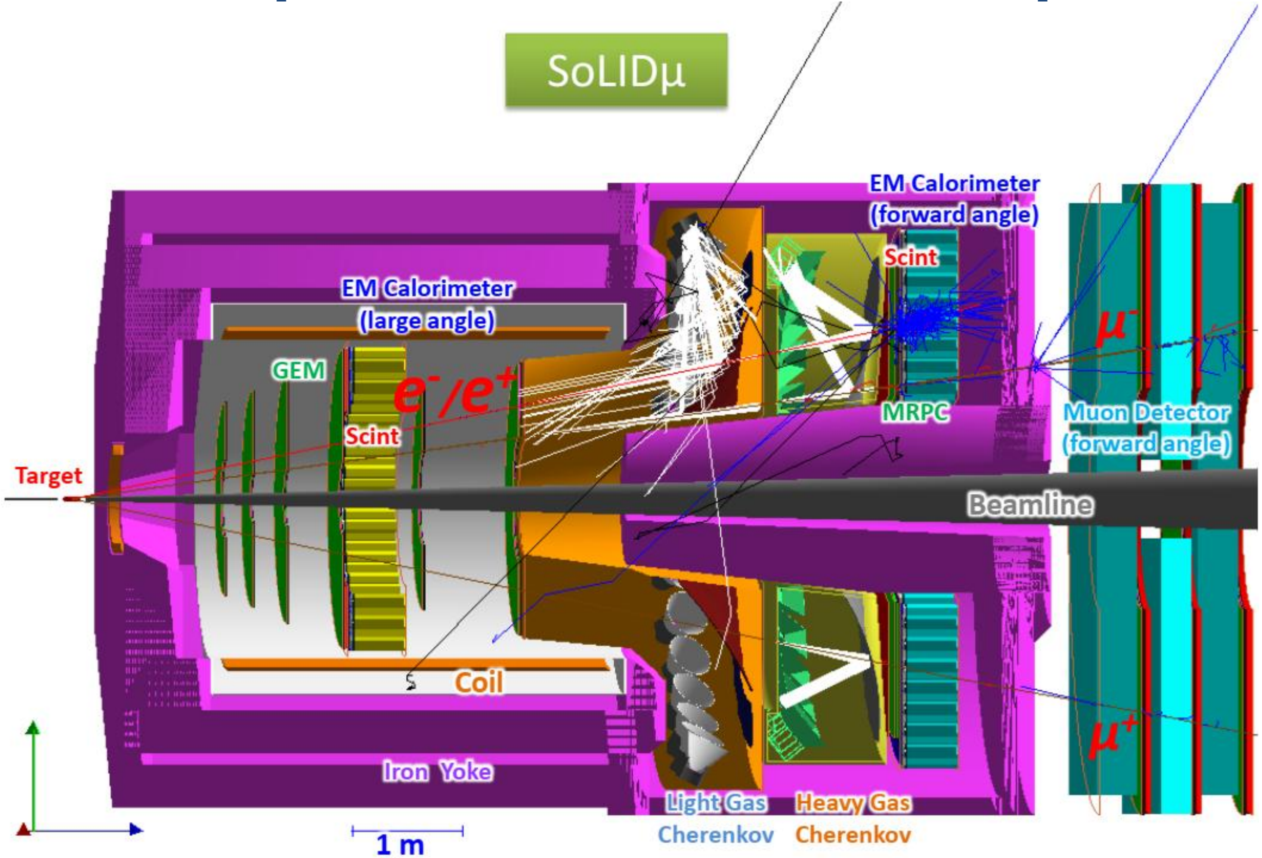

- SoLID can detect e^-, e^+, proton, pion
- Based on SoLID J/Psi and TCS setup (1.2e37/cm2/s) with forward angle muon detector added to form SoLIDμ spectrometer
- Sharing beam time with approved J/Psi and TCS di-e experiment
- Forward Angle (FA) covers 8.5-16.5deg and Large Angle (LA) covers 18-30deg

Forward Angle Muon Detector (FAMD)

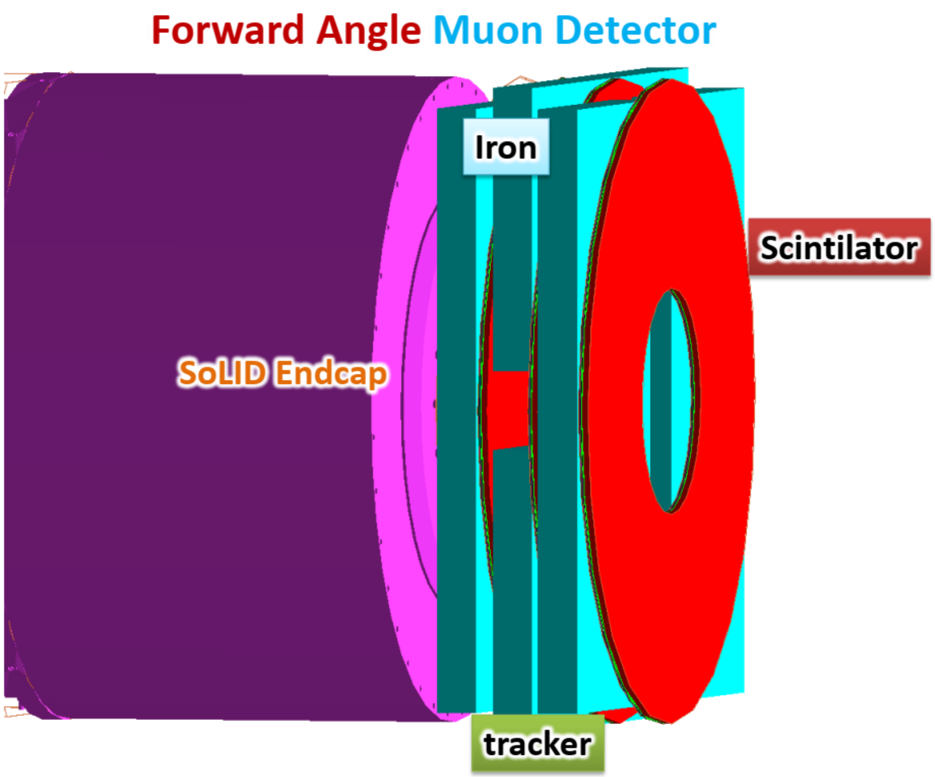

- 3 layers of iron+tracker+scintillator (Rin=1m, Rout=3m)
- Iron for pion blocking
- μRWell trackers to connect with tracks in SoLID inner GEM trackers
  - track resolution from SoLID inner trackers only
- scintillators for muon PID with pion suppression and trigger

Iron of FAMD

- Reuse 6 of CLEO octagon outer layer iron
- Each one is about 36x254x533cm
- No problem with space
- Field (<10G),force(<1N),torque(<2Nm) are small

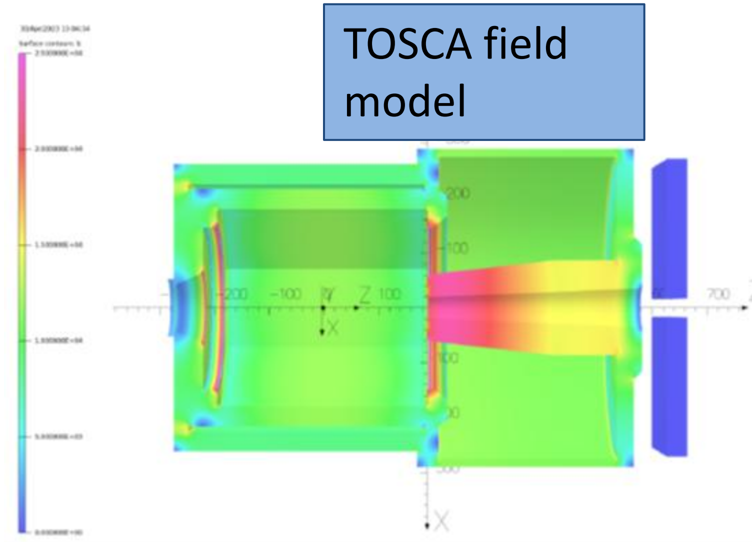

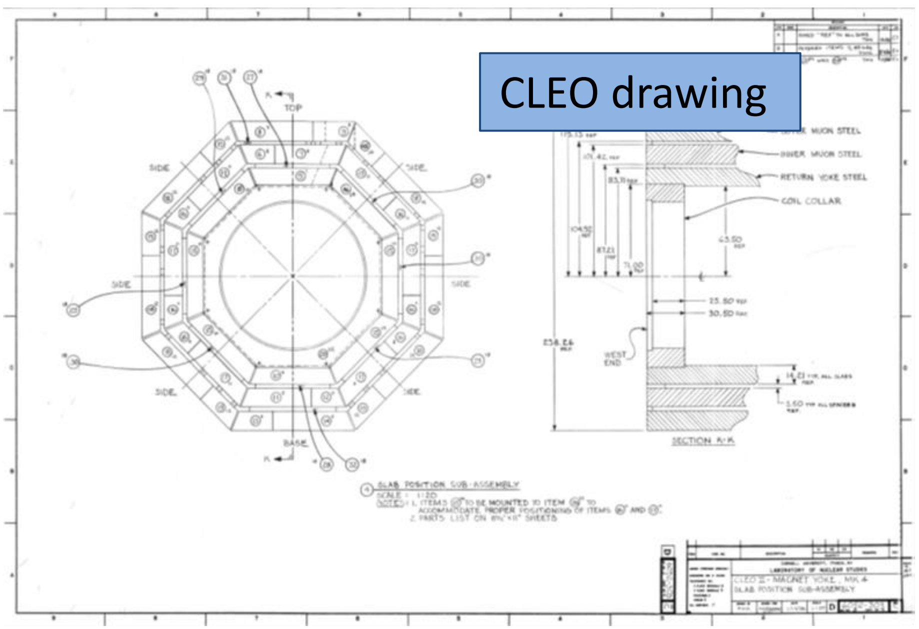

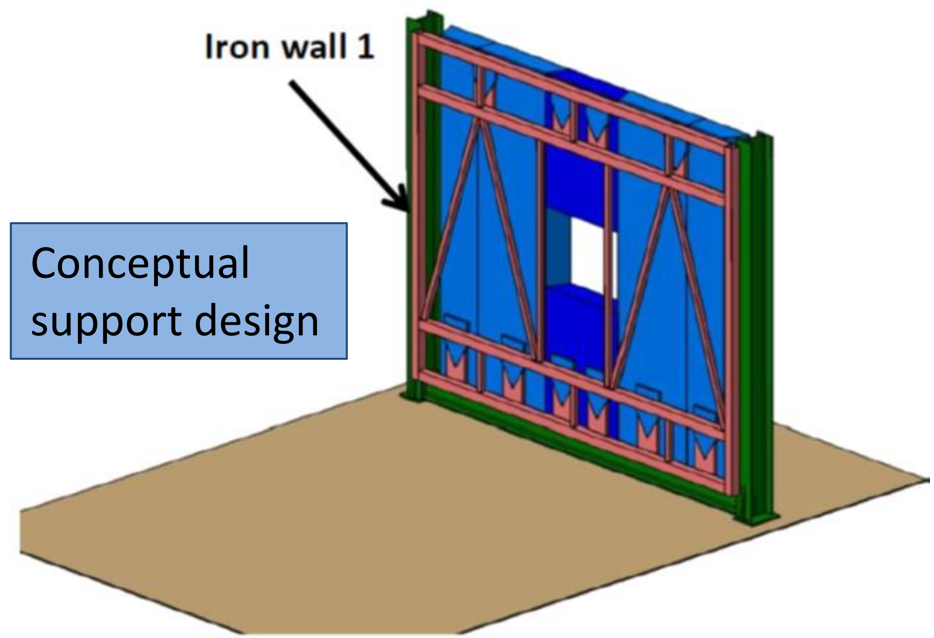

µRWell trackers of FAMD

- µRWell tracker with good rate capability and lower cost than GEM
- VMM electronics for readout
- 2D UV strips with capacitive charge sharing to have rate 30KHz/cm2 and position resolution of 1 mm

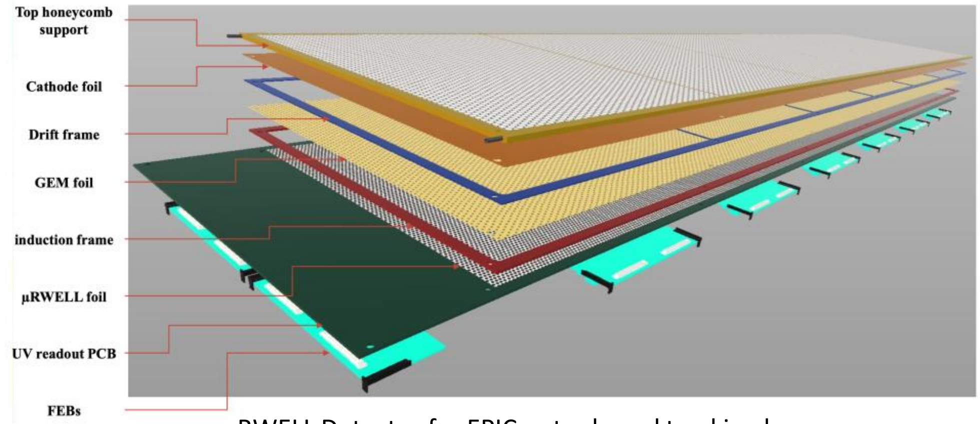

μRWELL Detector for EPIC outer barrel tracking layer

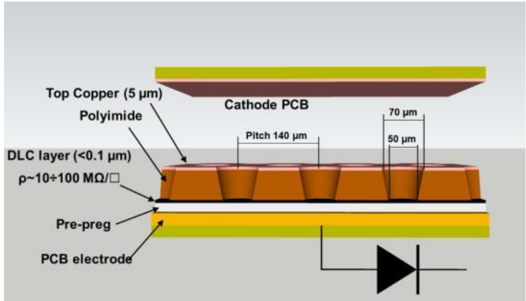

μRWELL Detector – G. Bencivenni *et al* 2019 *JINST* **14** P05014

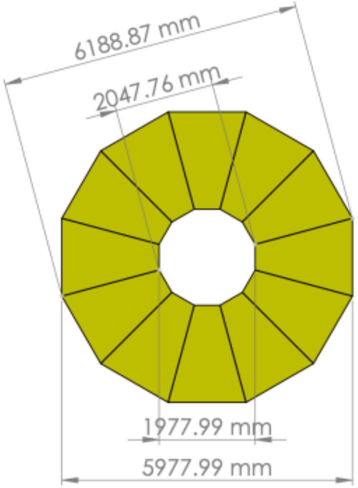

A plane of μRWELL detector

Scintillators of FAMD

- 3 layers of scintillator planes
- Each plane has 60 azimuthal segments
- Readout with light guide and PMTs from both inner and outer radial ends
- Design similar to CLAS12 forward scintillator and SoLID large angle scintillator with similar performance

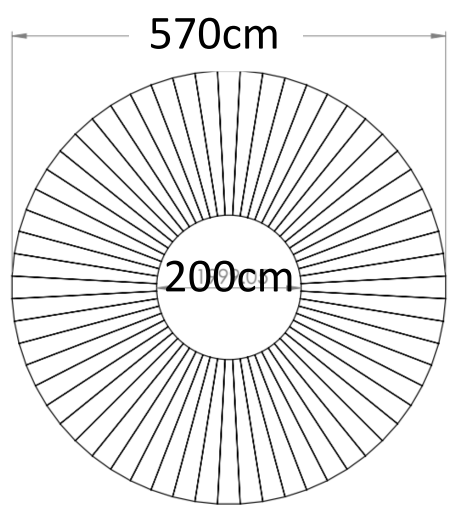

A plane of scintillator detector

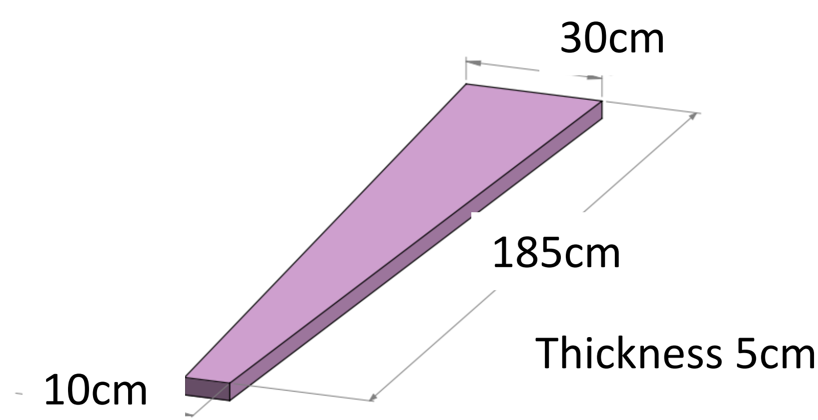

A module of scintillator detector

Event Acceptance

BH generator "grape-dilepton" used by HERA and verified by CLAS12

- Best topology 3-fold(e+mu+mu): scattered e- at FA+LA, both muons at FA, proton not detected
- Additional topology 4-fold(e+mu+mu+p): recoil proton at FA+LA (clean)

particle acceptance

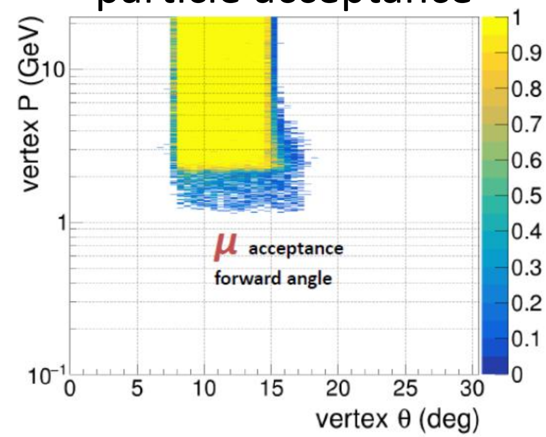

accepted BH 3-fold events

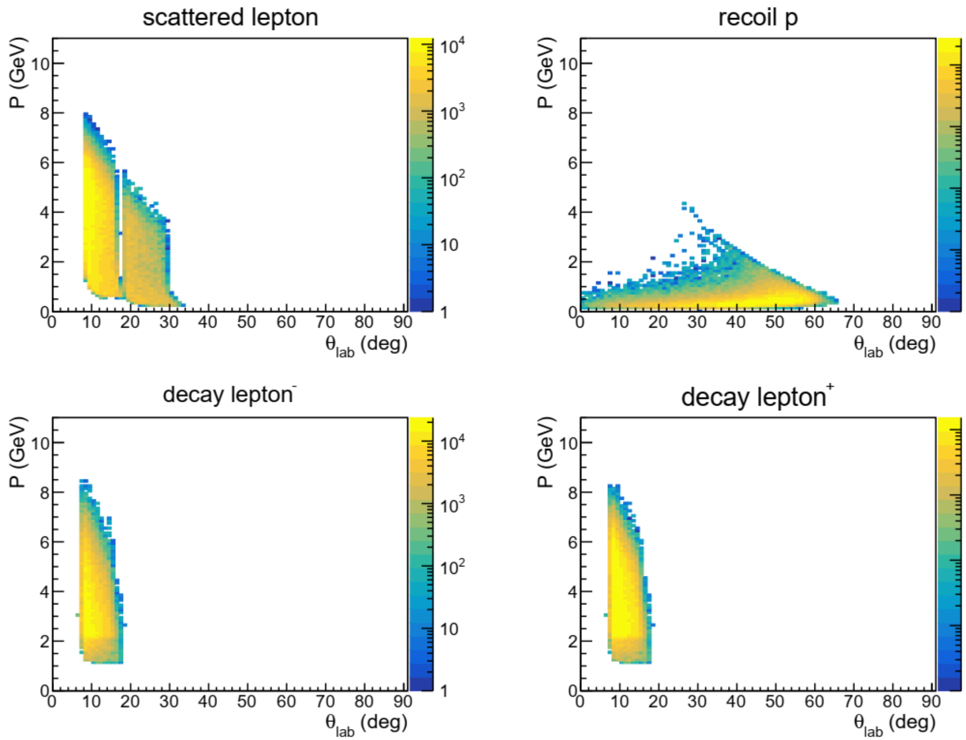

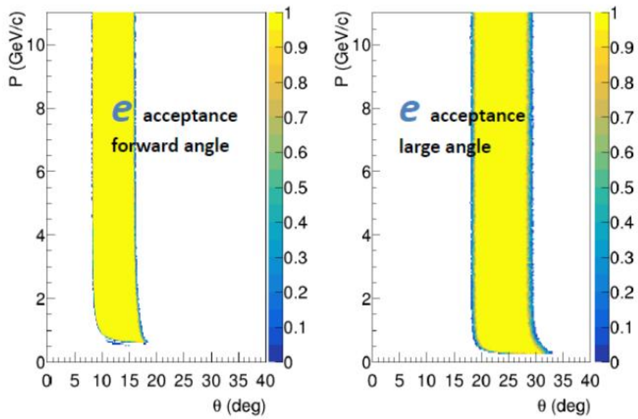

- full azimuthal coverage and large acceptance
- Solenoid field helps control systematics

Event Distribution

- 3-fold BH events covers a large kinematic range
- 0.7 overall detection efficiency
- Enough counts with 1.2e37/cm2/s luminosity and 100 days to have multidimensional binning

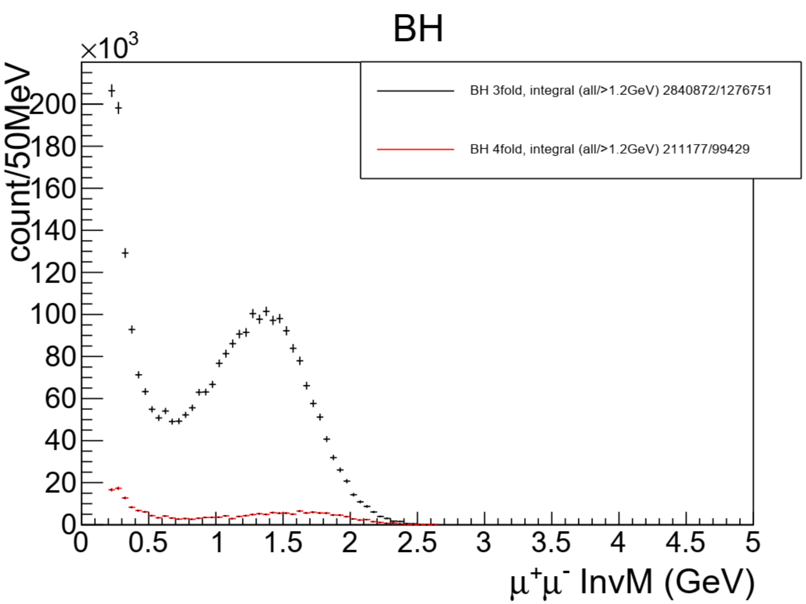

accepted BH 3-fold events

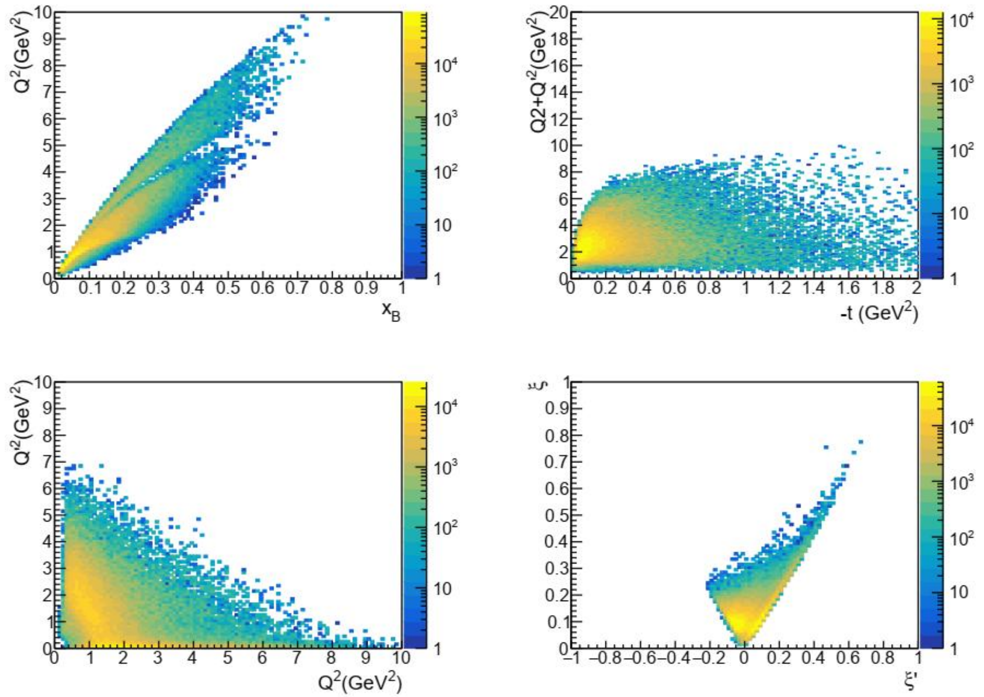

Exclusivity cut

- Both BH with 4 final particles (elastic) and more than 4 particles (quasi-elastic), generated by "grape-dilepton"
- Missing proton mass of 3 fold BH events with resolution from SoLID inner GEM trackers, for resonance free region (muon pair InvM>1.2GeV)
- 3-4% background after cutting MM>1.15GeV

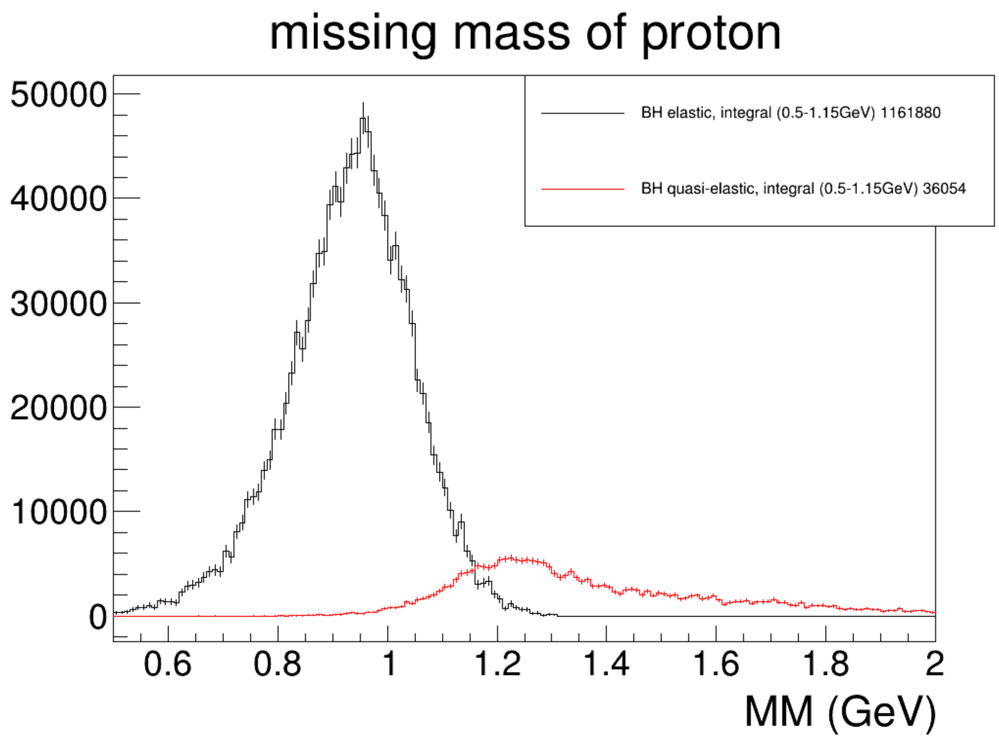

Pion blocking

- Geant4 simulation of pions from target with some probabilities creating hits at FAMD
- "pion hit probability", hits of charged particles entering each layer, used for FAMD background and trigger rate estimate
- "pion surviving probability", hits of pion and muon at the last layer of FAMD with tracks passing all SoLID inner GEM trackers, used for physics event rate estimation

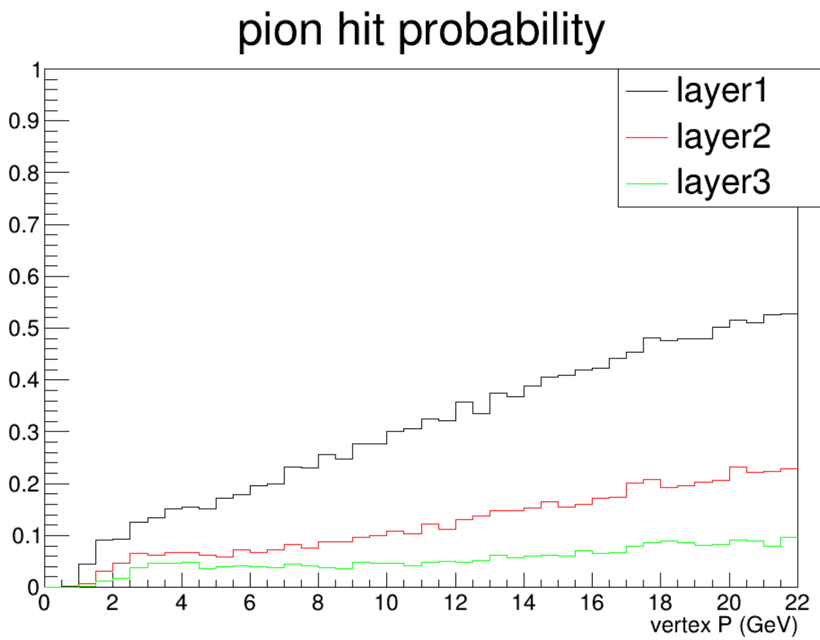

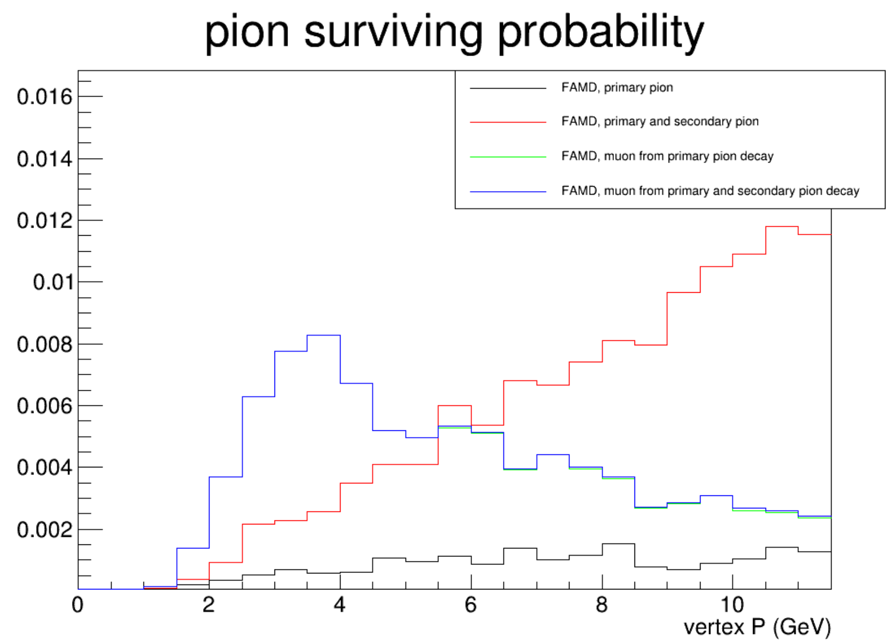

Pion suppression within FAMD

- Muons behave as Minimum Ionizing Particle (MIP)
- Pions often deposit more energy over 3 layers of scintillators.
- Use a moderate pion suppression factor 2 from energy cut

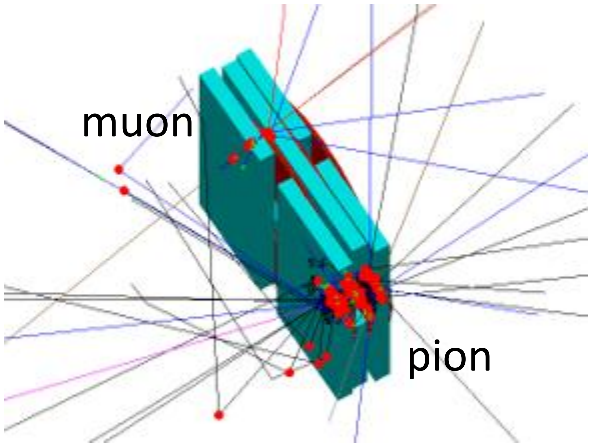

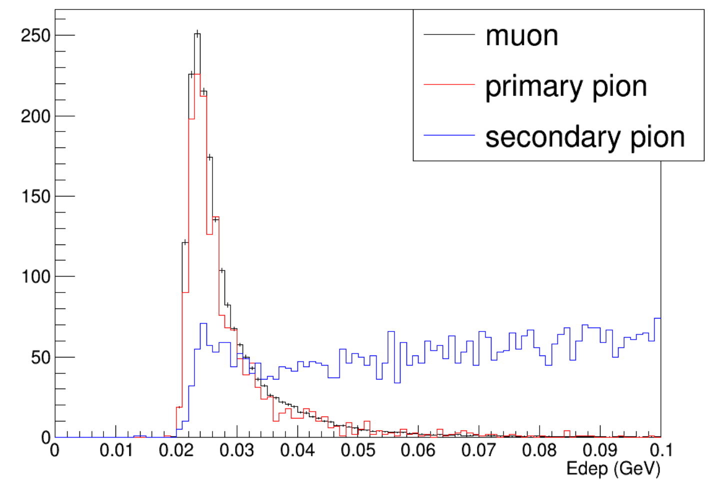

Single pion background

- Combining single pion generator "evgen_bggen" (pythia+MAID) events with "pion hit probability", study charged particle rate at 3 layers. Full simulation confirmed the result
- Single particle trigger 600khz rate with hits in all 3 layers of scintillators in nearby phi sectors
- Coincidence of two hits from 2 single particle trigger from 2 different phi sectors within 50ns time windows leads to 18khz final trigger rate
- Fake coin rate from single pion is below 1khz. BH di-muon events have two muons separated at least by 60 degrees in phi angle for the main physics region (muon pair InvM>1.2GeV)

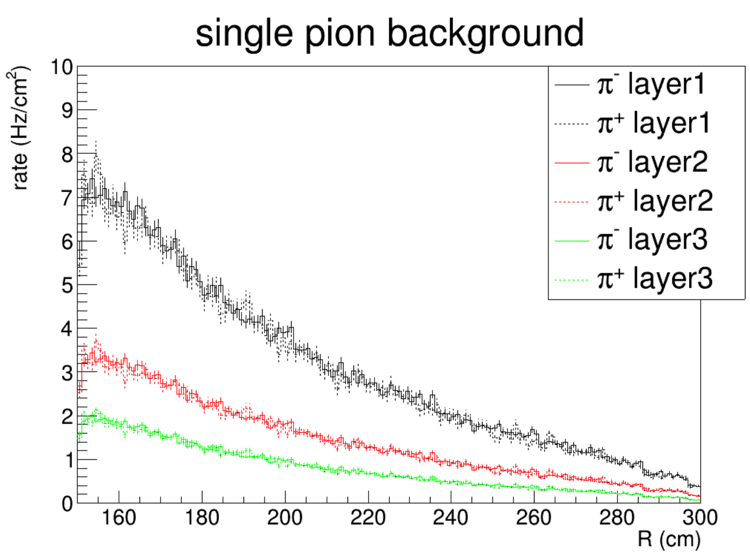

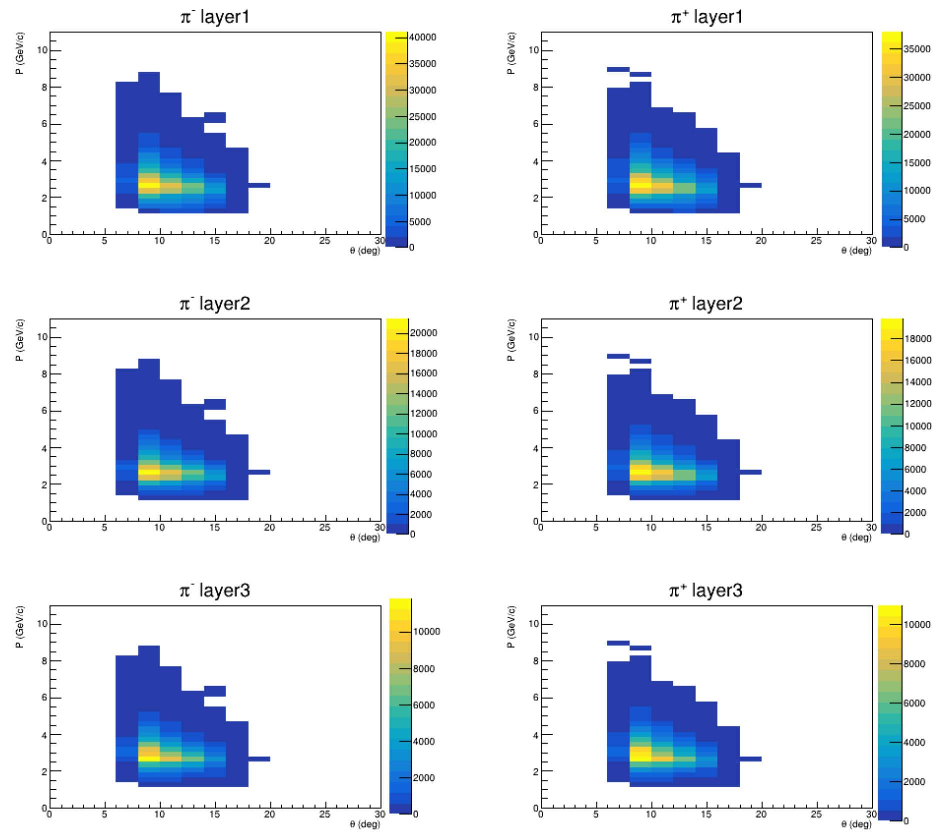

Two pion exclusive background

- Main physics background from two pion exclusive channel (missing mass cut won't reject it because pions and muons have similar mass)
- Combine event generator "twopeg" (fit to CLAS data) and "pion hit probability" with pion suppression factor 2, study "2pi" rate and compare to BH rate
- 5-7% background, while the channel be measured by the internal SoLID detector at the same time to control systematics

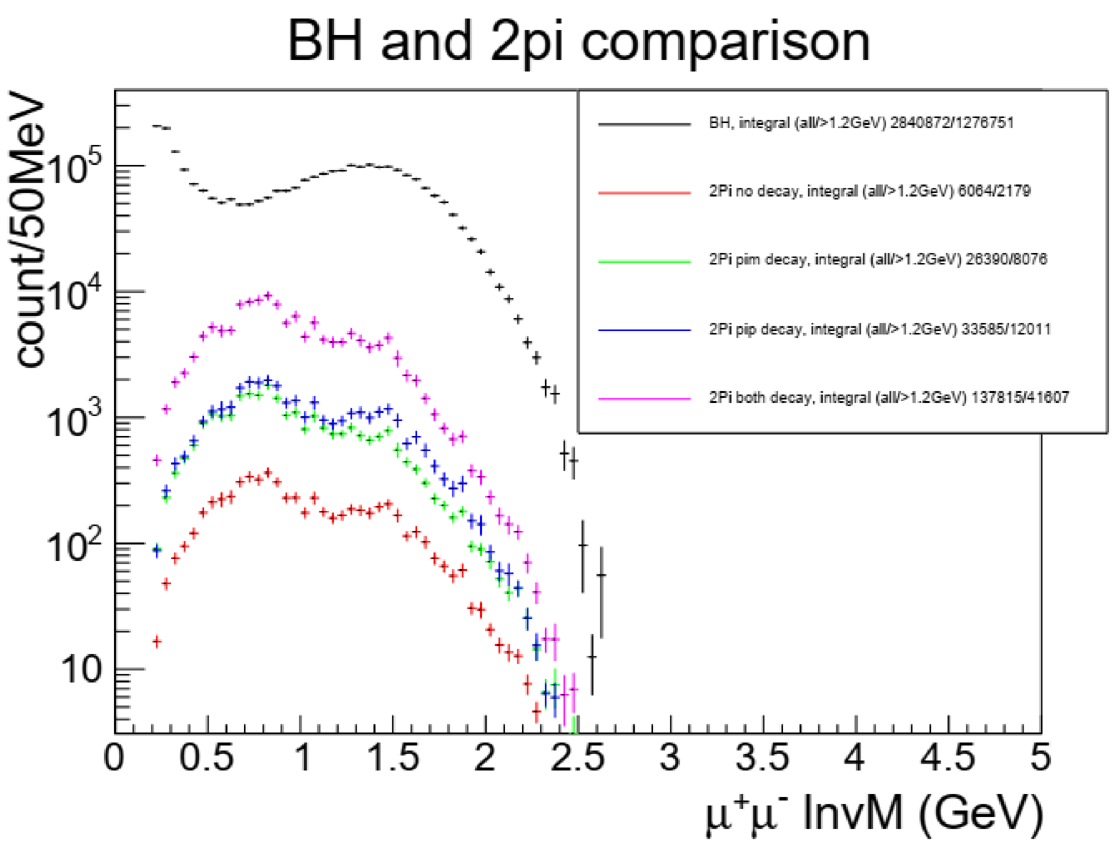

Experimental projection binning

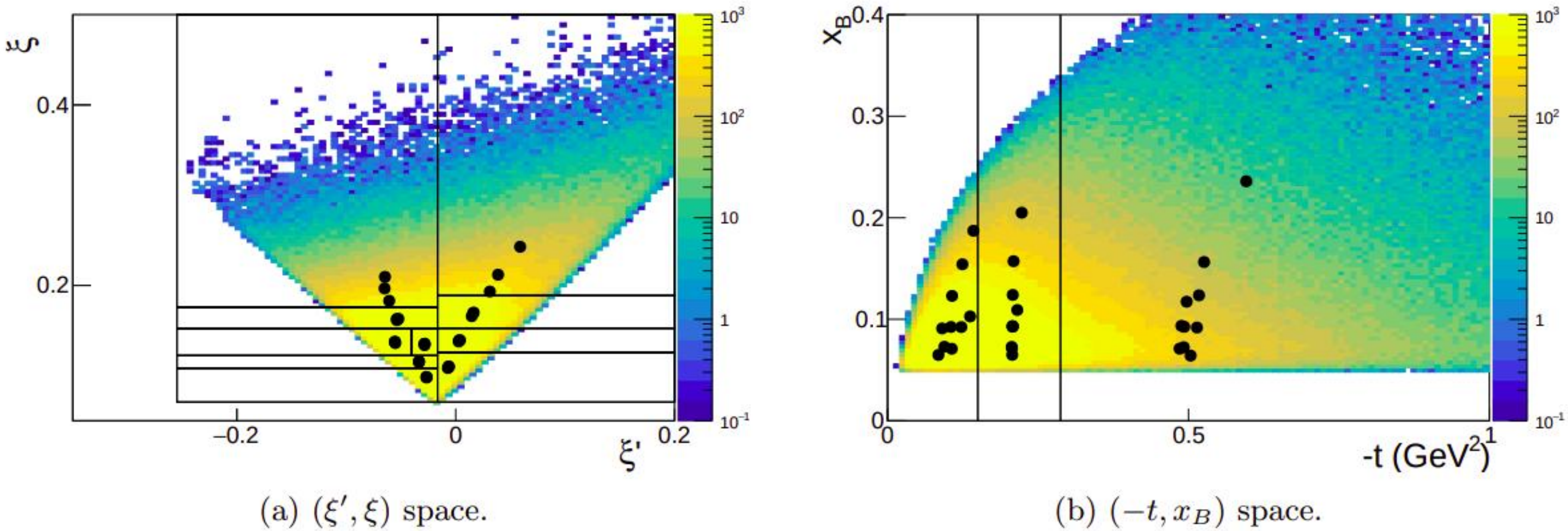

- 100 days would allow for measurements on a five-dimensional grid (ξ' ξ t x_B ϕ_μ)
- Covers both DVCS-like region ($\xi'>0$, $Q^2>Q'^2$) to TCS-like region ($\xi'<0$, $Q^2<Q'^2$)

BSA experimental projections

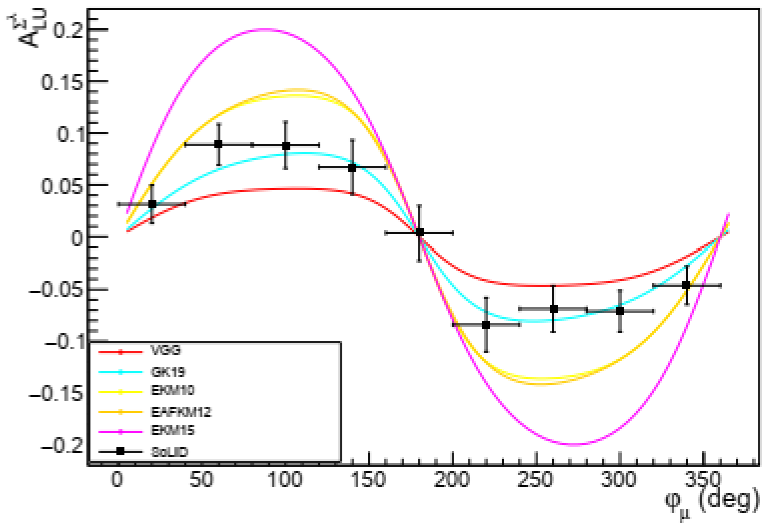

DVCS-like region

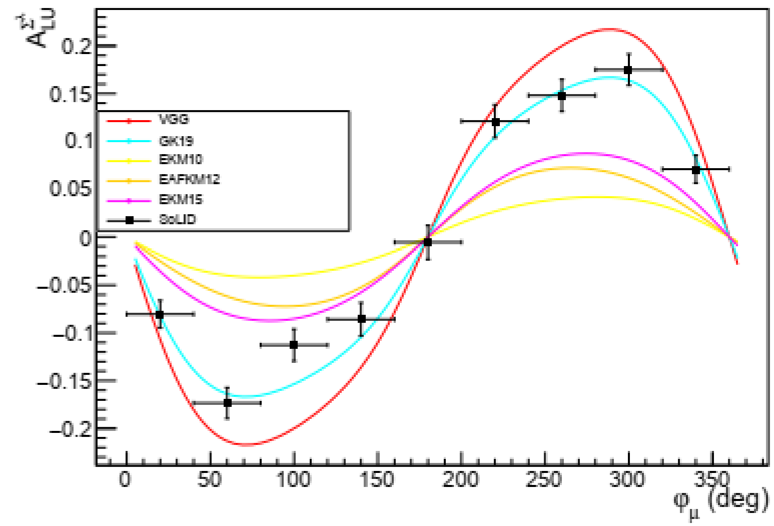

TCS-like region

arXiv:2502.02346

- First time measurement of the BSA sign change between the two regions
- Possibility to constrain GPD models

All projection plots include statistical and polarization errors

BSA experimental projections

All plots over the entire kinematic range

Bin	ξ' range	ξ range	t range (GeV^2)
1	$-0.255 < \xi' < 0$	$0.152 < \xi < 0.176$	$-5.541 < t < -0.287$
2			$-0.287 < t < -0.150$
3			$-0.150 < t < -0.020$
4		$0.176 < \xi < 0.739$	$-5.541 < t < -0.287$
5			$-0.287 < t < -0.150$
6			$-0.150 < t < -0.020$
7	$0 < \xi' < 0.512$	$0.071 < \xi < 0.126$	$-5.541 < t < -0.287$
8			$-0.287 < t < -0.150$
9			$-0.150 < t < -0.020$
10		$0.126 < \xi < 0.153$	$-5.541 < t < -0.287$
11			$-0.287 < t < -0.150$
12			$-0.150 < t < -0.020$
13		$0.153 < \xi < 0.189$	$-5.541 < t < -0.287$
14			$-0.287 < t < -0.150$
15			$-0.150 < t < -0.020$
16		$0.189 < \xi < 0.739$	$-5.541 < t < -0.287$
17			$-0.287 < t < -0.150$
18			$-0.150 < t < -0.020$
19	$-0.255 < \xi' < -0.017$	$0.071 < \xi < 0.108$	$-5.541 < t < -0.287$
20			$-0.287 < t < -0.150$
21			$-0.150 < t < -0.020$
22		$0.108 < \xi < 0.122$	$-5.541 < t < -0.287$
23			$-0.287 < t < -0.150$
24			$-0.150 < t < -0.020$
25	$-0.255 < \xi' < -0.040$	$0.122 < \xi < 0.152$	$-5.541 < t < -0.287$
			$-0.287 < t < -0.150$
			$-0.150 < t < -0.020$
	$) < \xi' < -0.017$	$0.122 < \xi < 0.152$	$-5.541 < t < -0.287$
			$-0.287 < t < -0.150$
			$-0.150 < t < -0.020$

Bin boundaries of the binning scheme shown in Fig. 24.

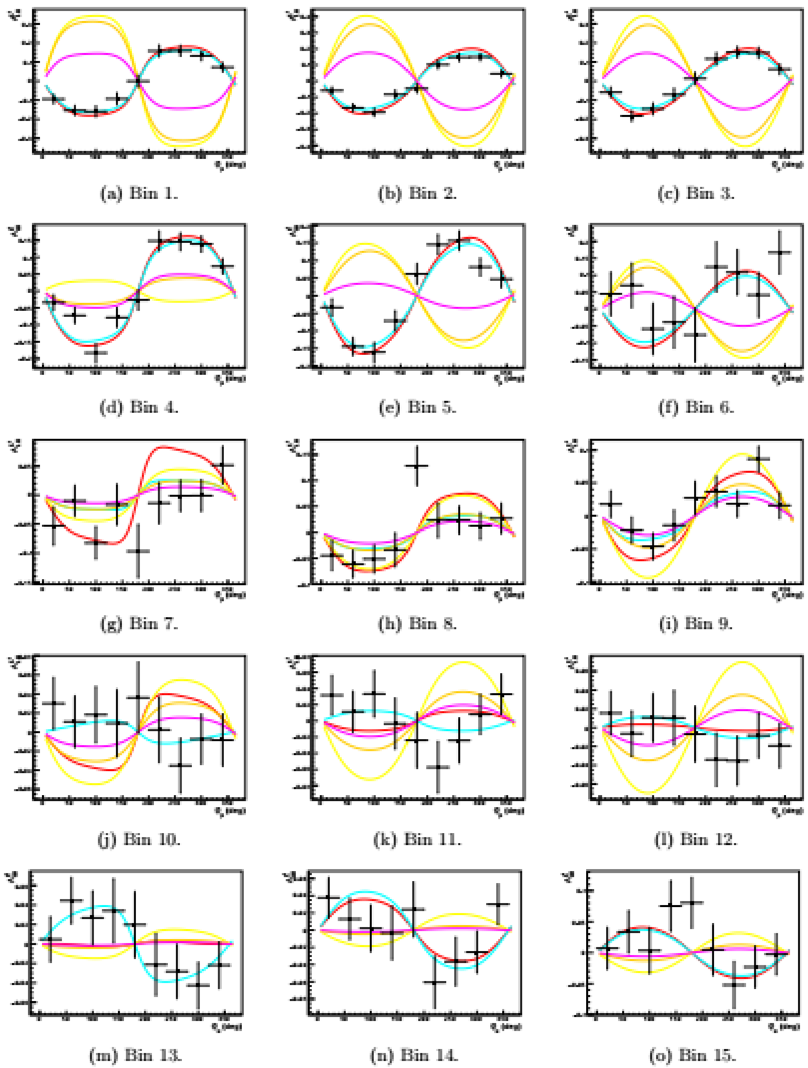

(a) Bin 1. (b) Bin 2. (c) Bin 3.
(d) Bin 4. (e) Bin 5. (f) Bin 6.
(g) Bin 7. (h) Bin 8. (i) Bin 9.
(j) Bin 10. (k) Bin 11. (l) Bin 12.
(m) Bin 13. (n) Bin 14. (o) Bin 15.

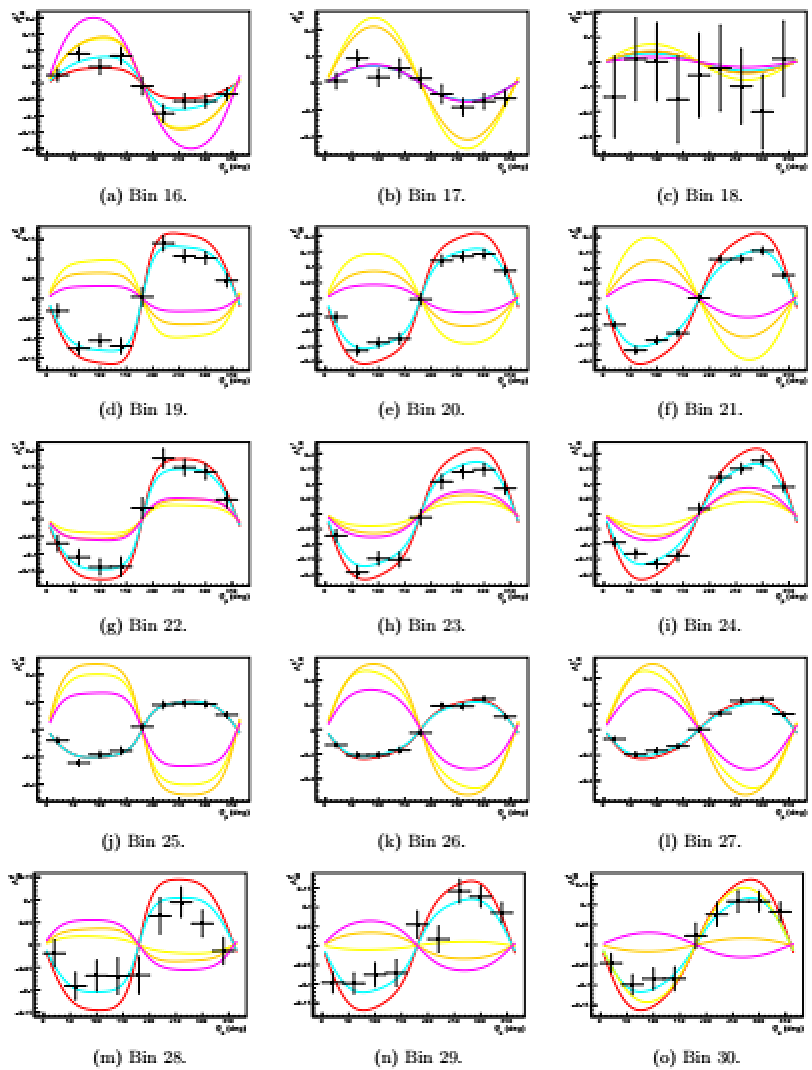

(a) Bin 16. (b) Bin 17. (c) Bin 18.
(d) Bin 19. (e) Bin 20. (f) Bin 21.
(g) Bin 22. (h) Bin 23. (i) Bin 24.
(j) Bin 25. (k) Bin 26. (l) Bin 27.
(m) Bin 28. (n) Bin 29. (o) Bin 30.

BSA experimental projections

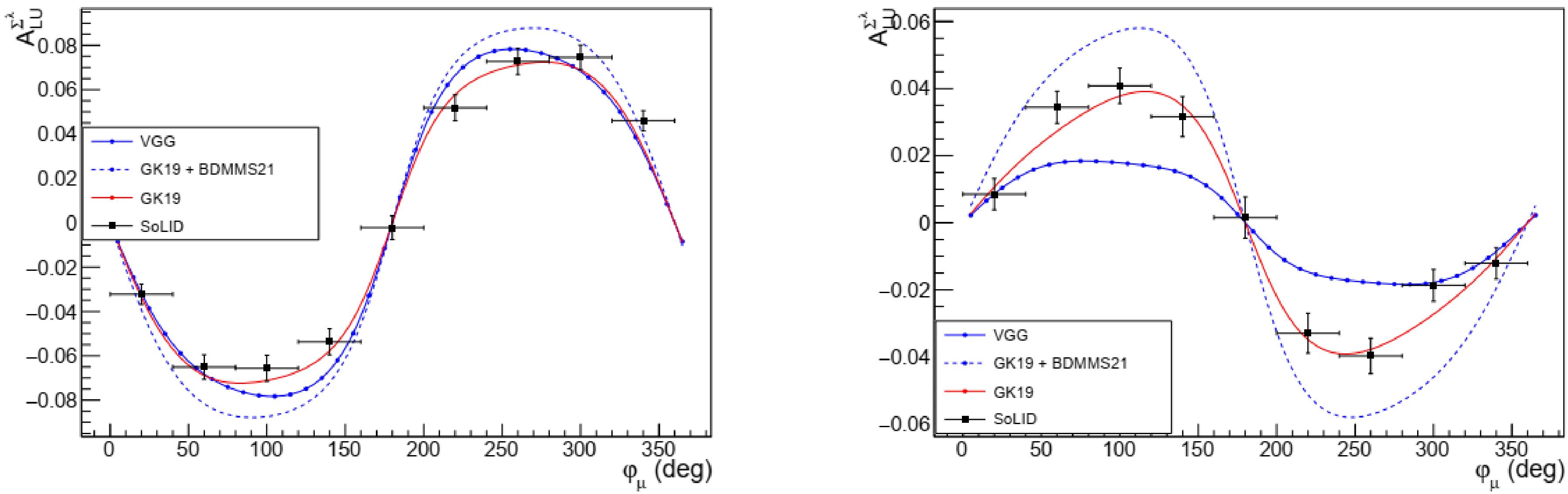

(a) $-0.1 < \xi' < -0.04$.

(b) $-0.04 < \xi' < 0.1$.

Figure 26: Projected exploratory TCS-like BSA measurements sensitive to shadow GPDs in the $0.3 < \xi < 0.4$ region.

First time exploratory measurement of BSA constraining shadow GPD models (a class of functions with null CFF and forward limit contributing to GPD solutions in the deconvolution problem)

Phys. Rev. D 103 (2021) 114019

µCA experimental projections

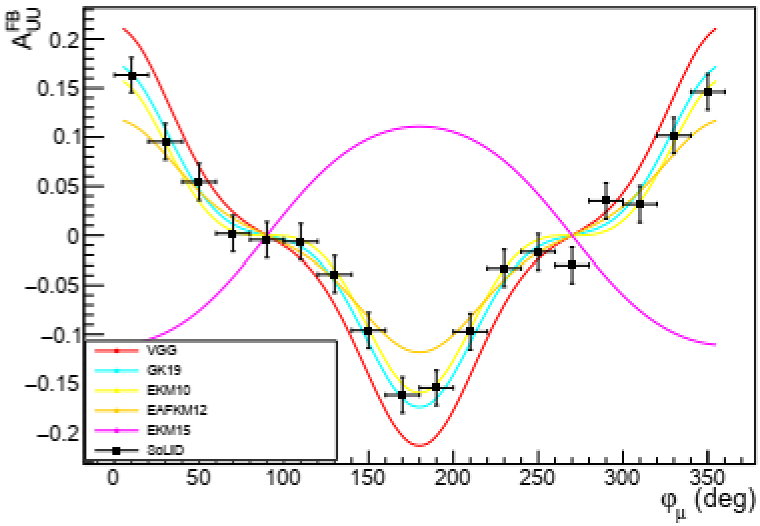

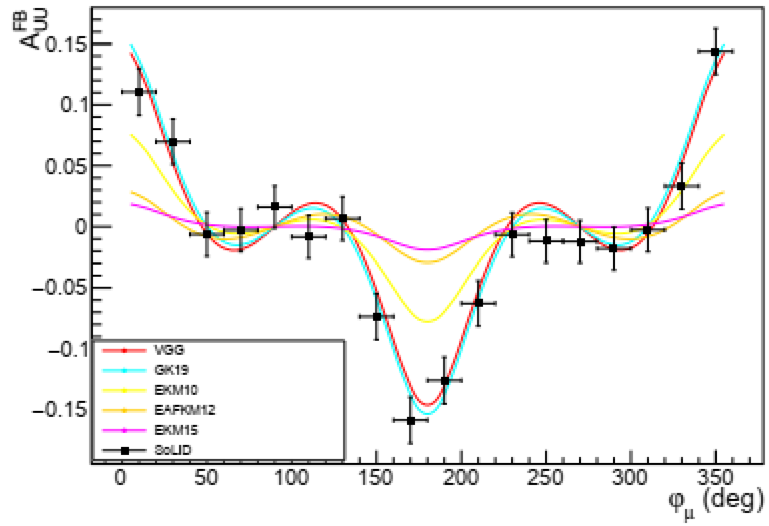

First time exploratory measurement of µCA to access the CFF real part with curvature change

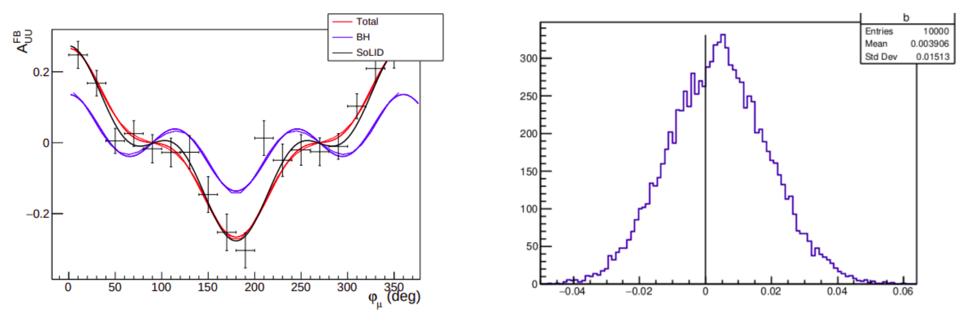

(a) μCA and the components entering the $\cos\varphi_\mu$ mo-

(b) Distribution of the $\cos\varphi_\mu$ moment of the μCA

$$A_{UU}^{\mu^\pm}(\varphi_\mu) = a_0 + a_1 \cos(\varphi) + a_3 \cos(3\varphi)$$

- known BH contribution is small in certain regions and can be subtracted
- µCA has contributions from cos(ϕ) and cos(3ϕ) modulations
- cos(ϕ) component can be extracted from fitting

Systematic effects

BSA systematics originates mainly from electron beam polarization, electron detection efficiency, and muon detection efficiency

$$\boxed{A_{LU}^{\Sigma\lambda} = \frac{1}{\lambda}\frac{Y_+ - Y_-}{Y_+ + Y_-}}$$

$$Y_\pm(\varphi_\mu) = \frac{1}{Q_\pm}\frac{1}{\Delta\Omega_e(\varphi_\mu)\,\Delta\theta_\mu(\varphi_\mu)}\int_0^{2\pi} d\phi \int_{\pi/4}^{3\pi/4} d\theta_\mu \sin(\theta_\mu)\frac{N_\pm(\varphi_\mu,\phi,\theta_\mu)}{\epsilon_e(\phi)\,\epsilon_\mu(\varphi_\mu,\theta_\mu)}$$

$$Y_\pm(\varphi_\mu) \equiv \sum_{i=1}^{N_\phi}\sum_{j=1}^{N_{\theta_\mu}}\frac{n_\pm^{ij}}{\epsilon_e^i\,\epsilon_\mu^j}$$

$$\boxed{\delta A_{LU}^{\Sigma\lambda} = \sqrt{\left[A_{LU}^{\Sigma\lambda}\right]^2\left(\frac{\delta\lambda}{\lambda}\right)^2 + \frac{1}{2\lambda^2}\frac{1}{N_\phi}\left(\frac{\delta\epsilon_e}{\epsilon_e}\right)^2 + \frac{1}{2\lambda^2}\frac{1}{N_{\theta_\mu}}\left(\frac{\delta\epsilon_\mu}{\epsilon_\mu}\right)^2}} \rightarrow \mathbf{0.04}$$

$\lambda = 0.85$

Bin independence hyptothesis

(N_ϕ, N_{θ_μ}) *are the kinematic dependent number of bins, typically (20,10)*

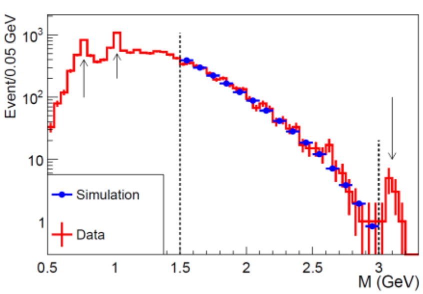

CLAS12 BH di-e data and sim comparison

Control systematics through reference channels

- SoLID will have crosssection measurement before this experiment
- For e- detection, use inclusive DIS and elastic measurements
- For muon detection, use both resonance and resonance free region and cross check both di-e and di-mu channels
- Pion channel measurement are also taken at the same time

Beam time request

Beam Energy (GeV)	Beam Current (uA)	Beam Requirements	Target Material	Target Thickness (cm)	Beam time (days)
11	3	polarized (>85%)	LH2	15	
Run Group Calibration time					10
Run Group Production time					50
Requested Production time					50
Total Time					110

- Main trigger on di-muon to take DDVCS, J/psi and TCS di-mu data at the same time
- Independent di-e trigger for approved J/psi and TCS di-e data taking at the same time
- Comprehensive program including muons and electrons within same runs. It can also help cross check systematics

Summary

This proposed experiment

- complement SoLID J/psi setup with a forward angle muon detector to form SoLIDμ spectrometer
- measure DDVCS in the di-muon channel
- share approved J/psi beamtime 60 days and request additional 50 days

Its physics impact

- first time measurement of DDVCS (mainly BSA and exploratory μCA) over a broad kinematic range
- first time to access GPD $|x| < \xi$ as input for models and global fitting

Proposal to PAC53 PR12-25-010

Proposal to JLab PAC 53

Double Deeply Virtual Compton Scattering with SoLIDμ spectrometer

Xinzhan Bai*, Alexandre Camsonne*†, Silviu Covrig Dusa, Kondo Gnanvo, Dave Mack, Michael McCaughan, and Richard Tyson

Thomas Jefferson National Accelerator Facility, Newport News, VA, USA

Juan-Sebastian Alvarado*, Raphaël Dupré, Adam Hobart, Dominique Marchand, Carlos Muñoz Camacho, Silvia Niccolai, and Eric Voutier*

Université Paris-Saclay, CNRS/IN2P3/IJCLab, Orsay, France

Haiyan Gao, Yining Liu, Bo Yu, Yi Yu, Zhiwen Zhao*, and Jingyi Zhou

Duke University, Durham, NC, USA

Keagan Bell, Debaditya Biswas, Marie Boër*, Gyang Chung, Mahmoud Gomina, Arna Ma, and Kemal Tezgin

Virginia Tech, Blacksburg, VA, USA

Garth Huber, Nathan Heinrich, Muhammad Junaid, Vijay Kumar, and Alicia Postuma

University of Regina, Regina, SK, Canada

Ronald Gilman

Rutgers University, Piscataway, NJ, USA

Nilanga Linayage, Huong Thi Nguyen, and Asar Ahmed

University of Virginia, Charlottesville, VA, USA

Yi Wang, Junhuai Xu, Zhihong Ye, Haojie Zhang, and Yaopeng Zhang

Tsinghua University, Beijing, China

Evaristo Cisbani

Istituto Superiore di Sanità, Roma, Italia

Guido Maria Urcioli

INFN, Sezione di Roma1, Roma, Italia

Vincenzo Bellini and Concetta Maria Sutera

Università di Catania, Catania, Italia

Anthony W. Thomas

ARC Special Research Centre for the Subatomic Structure of Matter (CSSM), University of Adelaïde, Adelaïde, Australia

Pierre Chatagnon[1], Maxime Defurne[1], Víctor Martínez-Fernández[1,2], Hervé Moutarde[1], and Franck Sabatié[1]

[1] *IRFU, CEA, Université Paris-Saclay, Gif-sur-Yvette, France*

[2] *Center for Frontiers in Nuclear Science, Stony Brook University, Stony Brook, NY, USA*

Malek Mazouz and Wassim Hamdi

Faculté des Sciences de Monastir, Département de Physique, Monastir, Tunisia

Whitney Armstrong, Sylvester Joosten, and Zein-Eddine Meziani

Argonne National Laboratory, Physics Division, Argonne, IL, USA

Thomas Hemmick

Stony Brook University, Stony Brook, NY, USA

Bernard Pire

Centre de Physique Théorique, CNRS, École polytechnique, I.P. Paris, Palaiseau, France

Pawel Sznajder and Jakub Wagner

National Centre for Nuclear Research, NCBJ, Warsaw, Poland

Johan A. Colorado-Caicedo

Centro de Investigacion y de Estudios Avanzados del Instituto Politecnico Nacional,San Pedro Zacatenco, Mexico City, Mexico

Sudip Bhattarai

Idaho State University,Pocatello, ID, USA

Nikos Sparveris, Hamza Atac, Suman Shrestha, and Mazmus. Ifat

Temple University, Philadelphia, PA, USA

Mostafa Elaasar

Southern University at New Orleans,New Orleans, LA,USA

Darko Androić

University of Zagreb, Faculty of Science, Zagreb, Croatia

Eric Fuchey

College of William & Mary, Williamsburg, Virginia, USA

Hem Bhatt

Mississippi State University, Mississippi State, MS, USA

Pawel Nadel-Turonski

University of South Carolina, Columbia, SC, USA

Xiaqing Li, Tianbo Liu, and Weizhi Xiong

Shandong University, Qingdao, Shandong, China

*: Co-spokesperson, †: Contact-spokesperson (camsonne@jlab.org)

and SoLID Collaboration

Spokesperson : Juan-Sebastian Alvarado, Alexandre Camsonne, Marie Boer, Eric Voutier, Xinzhan Bai, Zhiwen Zhao

Backup

GPD Parameterization

- **GPDs are universal quantities and reflect nucleon structure independently of the probing reaction.**
  - At leading twist–2, four quark chirality conserving GPDs for each quark type and gluon.
  - Because quark helicity is conserved in the hard scattering regime, the produced meson acts as a helicity filter.

$H^{q,g}(x,\xi,t)$ spin avg no hel. flip	$E^{q,g}(x,\xi,t)$ spin avg helicity flip
$\tilde{H}^{q,g}(x,\xi,t)$ spin diff no hel. flip	$\tilde{E}^{q,g}(x,\xi,t)$ spin diff helicity flip

- **Need a variety of Hard Exclusive Measurements to disentangle the different GPDs.**

Compton Scattering:

- Sensitive to all four GPDs.

Deep Exclusive Meson Production:

- Vector mesons sensitive to spin–average H E.
- Pseudoscalar sensitive to spin–difference $\tilde{H}$, $\tilde{E}$.

Nucleon Femtography

M. Burkardt PRD 62 (2000) 071503. M. Diehl EPJC 25 (2002) 223 A.V. Belitsky, D. Müller, NPA 711 (2002) 118c J.P. Ralston; B. Pire PRD 66 (2002) 111501

$$\boxed{\rho_H^q(x, \boldsymbol{b}_\perp) = \int \frac{d^2\boldsymbol{\Delta}_\perp}{(2\pi)^2}\, e^{i\boldsymbol{b}_\perp\cdot\boldsymbol{\Delta}_\perp} \left[H^q(x, 0, -\Delta_\perp^2) + H^q(-x, 0, -\Delta_\perp^2)\right]}$$

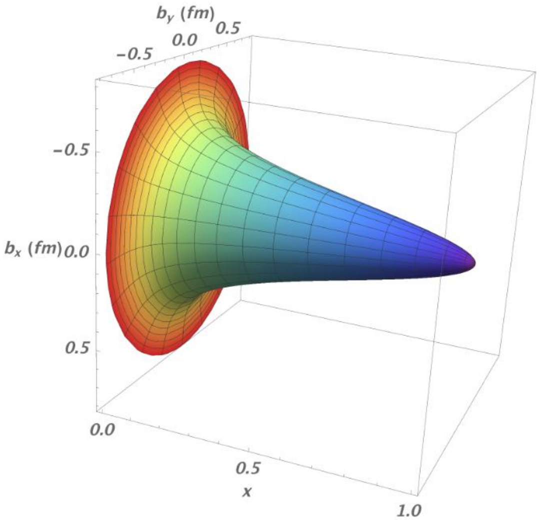

- The **transverse densities** of partons in nucleons and nuclei is related to the transverse momentum transfer ($-\Delta_\perp^2$) dependence of GPDs at **zero-skewness**.
- **DVCS** and **TCS cannot map out zero-skewness GPDs** over the **full physics phase space**.

The **experimental knowledge** of the **ξ-dependence** of GPDs at fixed longitudinal momentum fraction allows to **control** the **zero-skewness extrapolation** required for **nucleon imaging**.

R. Dupré, M. Guidal, M. Vanderhaeghen, PRD 95 (2017) 011501

Nucleon Spin

$$\lim_{t \to 0} \int_{-1}^{1} x \left[H^q(x,\xi,t) + E^q(x,\xi,t) \right] dx = J^q$$

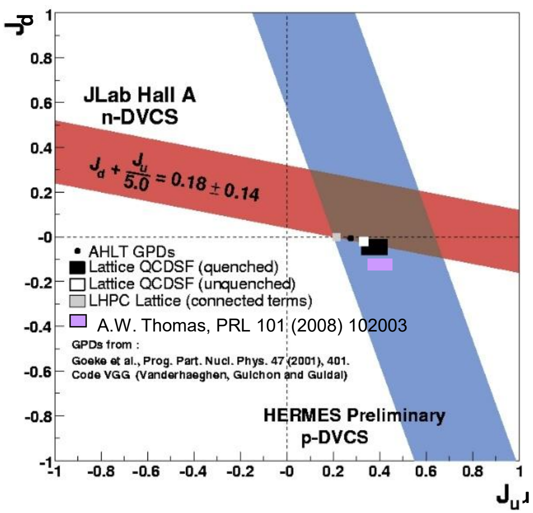

- The **total angular momentum of partons** inside the nucleon can be inferred from the Ji sum rule which involves the **forward limit** of the **first Mellin moment** of partons helicity conserving GPDs.
- **DVCS** and **TCS cannot access GPDs at $x \neq \xi$** over the **full physics phase space**.

The **experimental knowledge** of the **ξ-dependence** of GPDs at fixed longitudinal momentum fraction is a **mandatory step for** unraveling the **nucleon spin**.

Nucleon Forces

$$\boxed{\int_{-1}^{1} x \sum_q H^q(x,\xi,t)\ dx = M_2(t) + \frac{4}{5}\xi^2 d_1(t)}$$

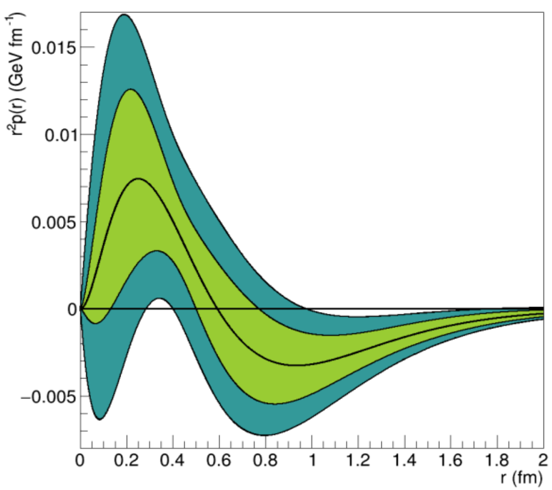

- The **skewness dependence** of the **first Mellin moment** of the GPD H provides an access to the **gravitational form factors** of the energy momentum tensor of the nucleon.
- **$e^{\pm}$-DVCS** and **TCS** offers another path via **dispersion relations**.

The **ξ-dependence** of GPDs reveals the **internal dynamics** of the nucleon.

V. Burkert, L. Elouadrhiri, F.-X. Girod, Nat. 557 (2018) 396; arXiv:2104.02031

Integrated Cross Section

5-fold observables obtained from the integration over the polar angle of the muon and the azimuthal angle of initial virtual photon or final virtual photon are required, also minimizing the contribution of the BH_2 process

DVCS-like xs (integral of ϕ_μ)

$$d^5\sigma^\lambda(\phi) \equiv \frac{d^5\sigma^\lambda(\phi)}{dx_B\, dy\, dt\, dQ'^2\, d\phi} = \int_0^{2\pi} d\varphi_\mu \int_{\pi/2-\theta_0}^{\pi/2+\theta_0} d\theta_\mu \sin(\theta_\mu)\, \frac{d^7\sigma^\lambda(\phi,\theta_\mu,\phi_\mu)}{dx_B\, dy\, dt\, d\phi\, dQ'^2\, d\Omega_\mu}$$

$$d^5\sigma^\lambda = d^5\sigma_{BH_1} + d^5\sigma_{BH_2} + d^5\sigma_{DDVCS} + d^5\sigma_{\mathcal{I}_1} + \lambda\, d^5\widetilde{\sigma}_{\mathcal{I}_1} = d^5\sigma_{UU} + \lambda\, d^5\sigma_{LU}$$

TCS-like xs (integral over ϕ)

$$d^5\Sigma^\lambda(\varphi_\mu) \equiv \frac{d^5\sigma^\lambda(\varphi_\mu)}{dx_B\, dy\, dt\, dQ'^2\, d\varphi_\mu} = \int_0^{2\pi} d\phi \int_{\pi/2-\theta_0}^{\pi/2+\theta_0} d\theta_\mu \sin(\theta_\mu)\, \frac{d^7\sigma^\lambda(\phi,\theta_\mu,\phi_\mu)}{dx_B\, dy\, dt\, d\phi\, dQ'^2\, d\Omega_\mu}$$

$$d^5\Sigma^\lambda = d^5\Sigma_{BH_1} + d^5\Sigma_{BH_2} + d^5\Sigma_{BH_{12}} + d^5\Sigma_{DDVCS} + d^5\Sigma_{\mathcal{I}_1} + d^5\Sigma_{\mathcal{I}_2} + \lambda\, d^5\widetilde{\Sigma}_{\mathcal{I}_2} = d^5\Sigma_{UU} + \lambda\, d^5\Sigma_{LU}$$

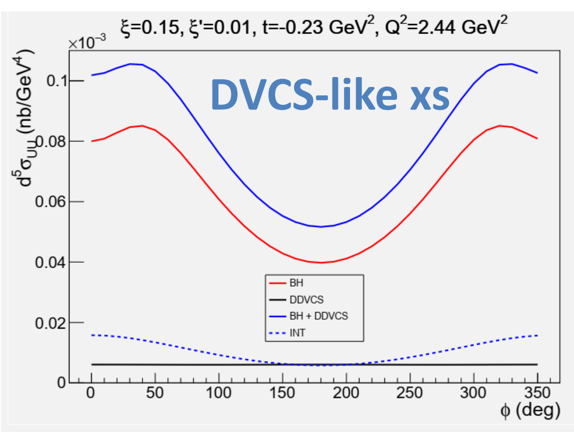

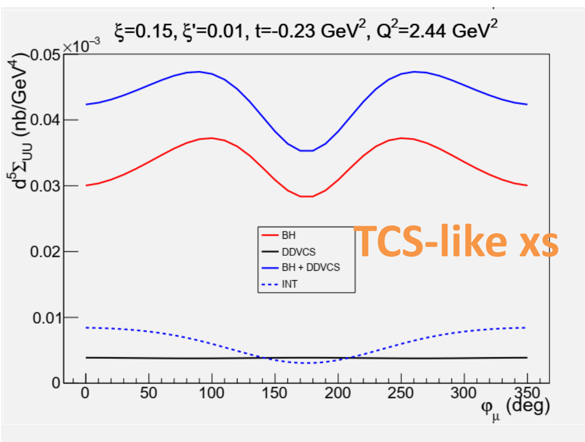

Our study focuses on using TCS-like xs for projection

Muon Charge Asymmetry

aka Forward Backward Asymmetry

$$A_{UU}^{FB}(\varphi_\mu) = \frac{d^5\Sigma_{UU}(\varphi_{\mu^-}) - d^5\Sigma_{UU}(\varphi_{\mu^-}+\pi)}{d^5\Sigma_{UU}(\varphi_{\mu^-}) + d^5\Sigma_{UU}(\varphi_{\mu^-}+\pi)} = \frac{d^5\Sigma_{UU}(\varphi_{\mu^-}) - d^5\Sigma_{UU}(\varphi_{\mu^+})}{d^5\Sigma_{UU}(\varphi_{\mu^-}) + d^5\Sigma_{UU}(\varphi_{\mu^+})} = A_{UU}^{\mu^\pm}(\varphi_\mu)$$

$$\begin{aligned} d^5\Sigma_{UU}(\varphi_{\mu^-}+\pi) &= \int_0^{2\pi} d\phi \int_{\pi/2-\theta_0}^{\pi/2+\theta_0} d\theta_{\mu^-} \sin(\theta_{\mu^-}) \frac{d^7\sigma^0(\phi, \pi-\theta_{\mu^-}, \varphi_{\mu^-}+\pi)}{dx_B\, dy\, dt\, d\phi\, dQ'^2\, d\Omega_{\mu^-}} \\ &= \int_0^{2\pi} d\phi \int_{\pi/2-\theta_0}^{\pi/2+\theta_0} d\theta_{\mu^+} \sin(\theta_{\mu^+}) \frac{d^7\sigma^0(\phi, \theta_{\mu^+}, \varphi_{\mu^+})}{dx_B\, dy\, dt\, d\phi\, dQ'^2\, d\Omega_{\mu^+}} = d^5\Sigma_{UU}(\varphi_{\mu^+}) \end{aligned}$$

$$A_{UU}^{\mu^\pm}(\varphi_\mu) = \frac{d^5\Sigma_{BH_{12}} + d^5\Sigma_{\mathcal{I}_2}}{d^5\Sigma_{BH_1} + d^5\Sigma_{BH_2} + d^5\Sigma_{DDVCS} + d^5\Sigma_{\mathcal{I}_1}}$$

$$d^5\Sigma_{\mathcal{I}_2} \propto -\frac{\xi'}{\xi}\Re\mathfrak{e}\left[F_1\mathcal{H} + \frac{\xi^2}{\xi'}(F_1+F_2)\tilde{\mathcal{H}} - \frac{t}{4M_N^2}F_2\mathcal{E}\right]$$

- Access to the real part of CFFs (no existing dispersion relation)
- **μCA** predicted to have **significant amplitude** and rich **harmonic composition**, like the forward-backward asymmetry of TCS
- **Curvature change** is a highly-discriminating feature for models
- **DDVCS μCA** access a CFF combination **different** from **BSA**. This feature **distinguishes DDVCS** from DVCS and TCS.

$$A_{UU}^{\mu^\pm}(\varphi_\mu) = a_0 + a_1\cos(\varphi) + a_3\cos(3\varphi)$$

$$\frac{d^4\sigma_{INT}}{dQ'^2dtd\Omega} = -\frac{\alpha_{em}^3}{4\pi s^2}\frac{1}{-t}\frac{m_p}{Q'}\frac{1}{\tau\sqrt{1-\tau}}\frac{L_0}{L}[\cos(\phi)\frac{1+\cos^2(\theta)}{\sin(\theta)}\mathrm{Re}\tilde{M}^{--} \cancel{-\cos(2\phi)\sqrt{2}\cos(\theta)\mathrm{Re}\tilde{M}^{0-}} + \cos(3\phi)\sin(\theta)\mathrm{Re}\tilde{M}^{+-} + O(\frac{1}{Q'})],$$

Muon Detector Tracker

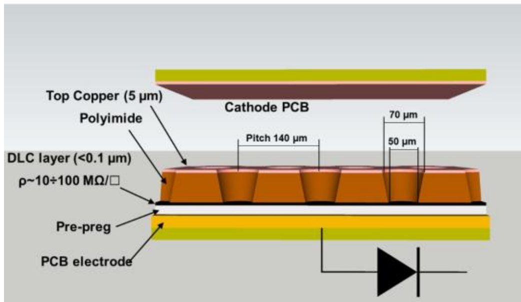

μRWELL Detector – G. Bencivenni *et al* 2019 *JINST* **14** P05014

- Utilize μRWELL detectors for muon tracking layers
  - Current μRWELL detector rate capability – ~200 KHz/cm^2 (High-rate version in development – 10 MHz/cm^2)
  - Discharge resistant thanks to integrated DLC layers – a huge improvement on electronics stability – less interruption on DAQ during running
  - No spacers needed compared with GEM detectors – no dead area
- A similar technology adopted by EIC
  - Our muon detector unit would be roughly in the same size as EIC prototypes
  - Total cost (3 complete layers covering a total of 75 m^2) around 900K

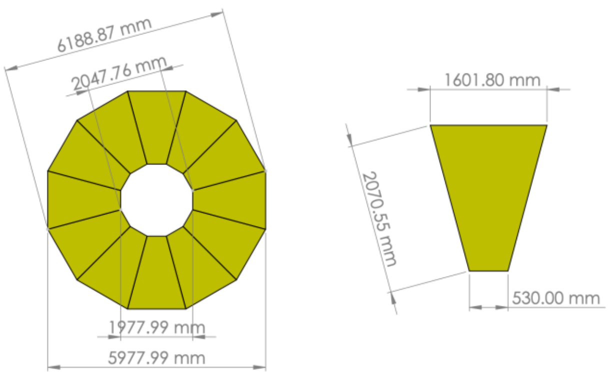

A plane of μRWELL detectors for muon detection

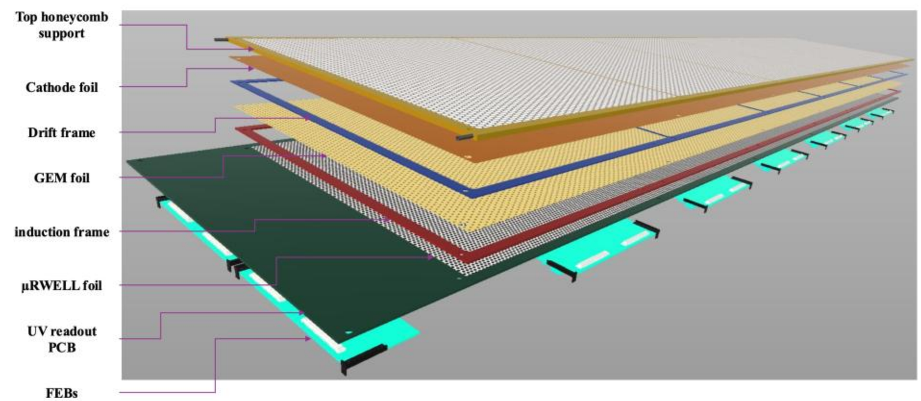

μRWELL Detector for EPIC outer barrel tracking layer

Muon Detector Tracker

- Use capacitive charge sharing technique to reduce total readout channels while maintain the same space resolution
- Works for all readout patterns – strip, pad, zigzag, …

With Capacitive charge sharing:

- Space resolution : 1 mm
- Total readout channel can be reduced to around 22K for all 3 layers combined
- Detector rate will be determined by the final readout strip width, larger strip width leads to lower detector rate capability
- For 22K readout channels, 1 mm space resolution, with capacitive charge sharing technique – rate capability: $\sim 30\ KHz/cm^2$ (assume 300 ns signal integral time)

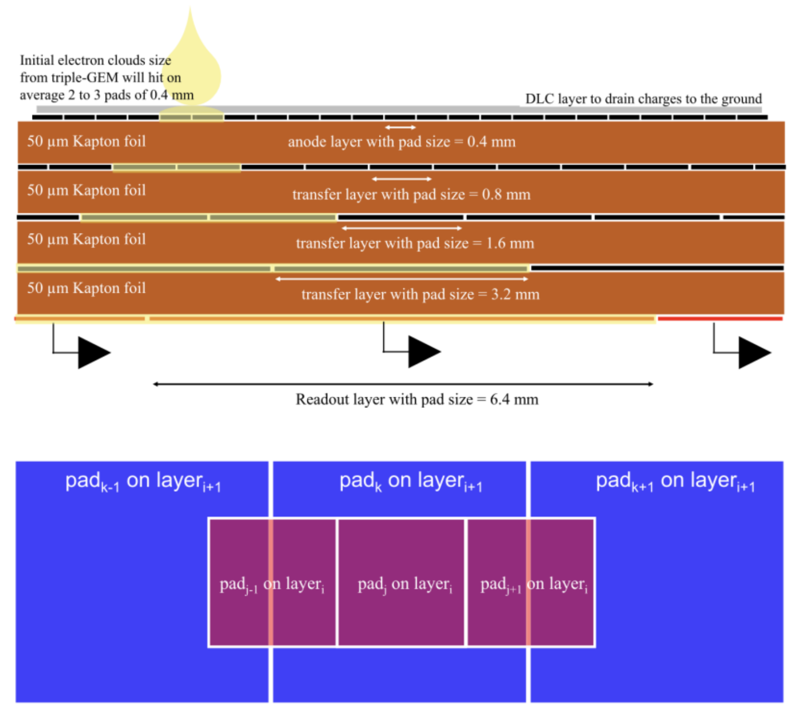

Concept for capacitive charge sharing – K. Gnanvo *et al, Nuclear Inst. and Methods in Physics Research, A 1047 (2023) 167782*

SoLIDμ vs μCLAS12

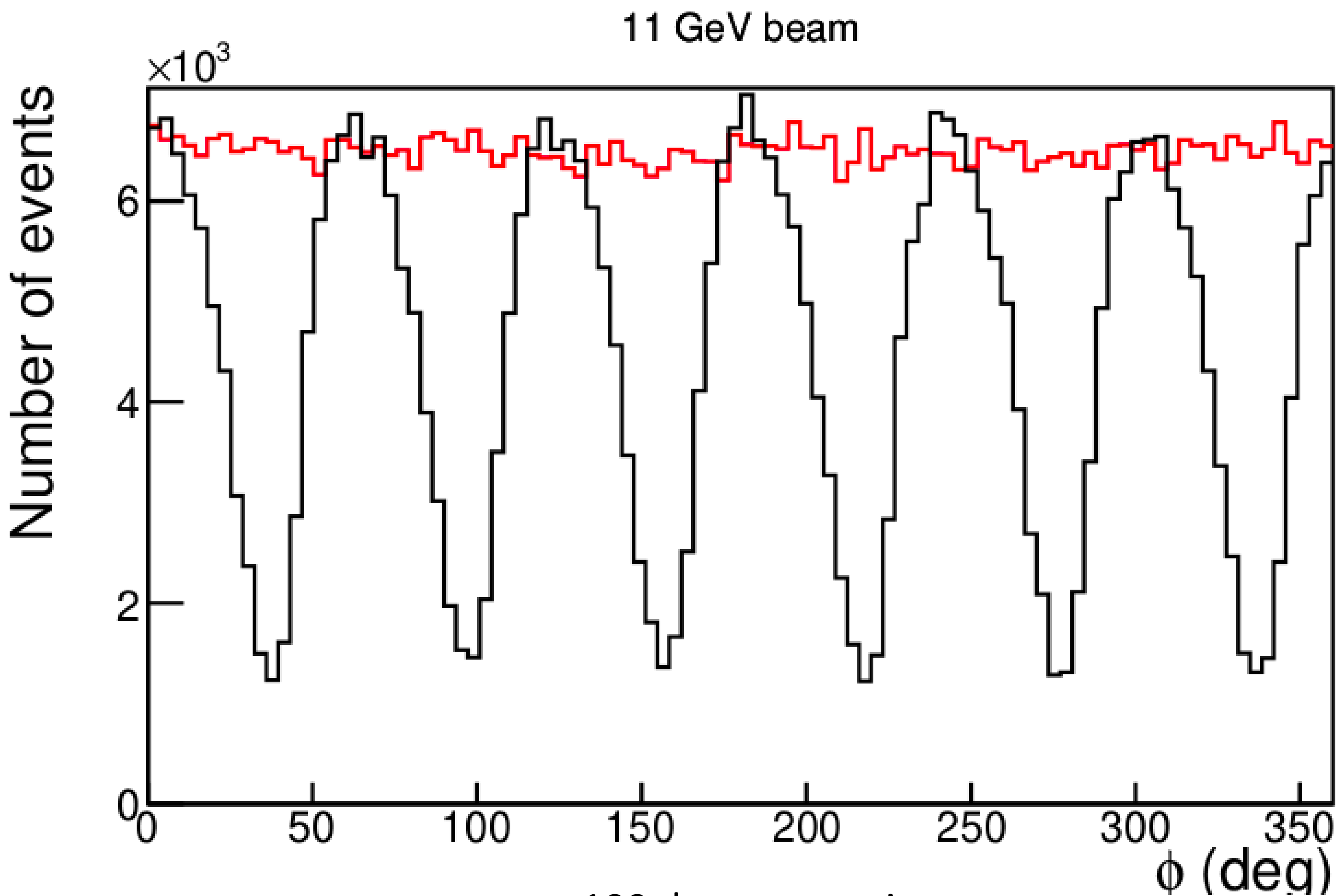

100 days comparison

SoLIDμ vs μCLAS12

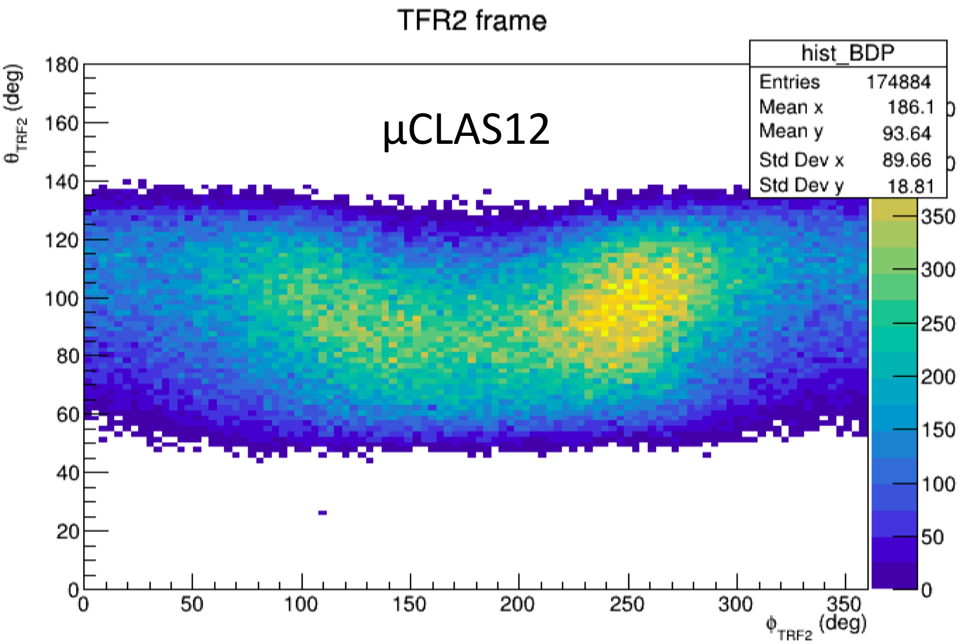

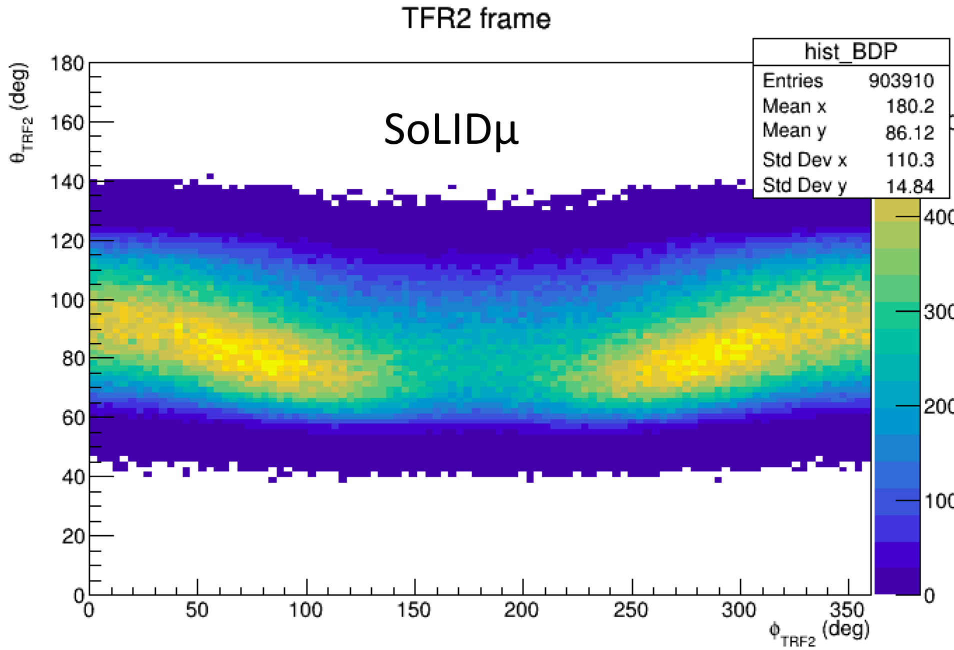

- Angles in the muon center-of-mass frame
- Larger coverage with SoLIDμ

BH and trigger

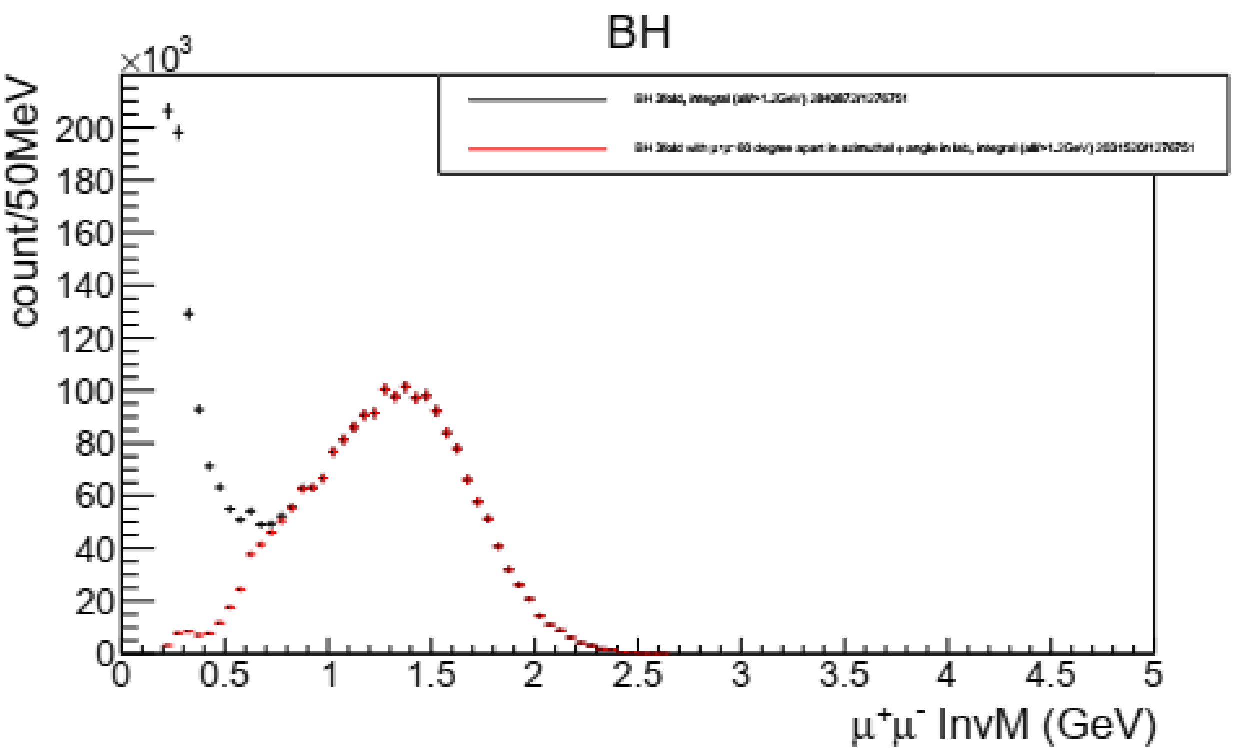

Systematic effects

- Systematics of the measurements will be controlled via **simulations** and the measurement of **reference processes**. The **solenoidal field** and the **symmetrical configuration** of SoLIDμ offer further cross-checks
- **Muon solid angle** : extensive simulations based on the **SoLIDμ GEANT4 model** ($\delta\Delta\theta_{\mu}/\Delta\theta_{\mu}{\sim}3\%$)
- **Electron detection efficiency** : measurement of **DIS** and **elastic** electron **scattering** ($\delta\epsilon_{e}/\epsilon_{e}{\sim}7\%$)
- **Muon detection efficiency** : measurement of **Bethe-Heitler** and comparison of the $\boldsymbol{e^{\pm}}$ and $\boldsymbol{\mu^{\pm}}$ **decay** of specific meson (ϕ, J/Ψ) ($\delta\epsilon_{\mu}/\epsilon_{\mu}{\sim}15\%$)

Background asymmetry

- signal channel asymmetry As=0.1 and rate Rs
- background channel asymmetry Ab=0.5 and rate Rb
- Background/signal rate Rb/Rs=0.05 with error ER=0.01
- Rel_Error of As = (As-Ab)/(1-Rb/Rs)^2*ER/As

  = (0.1-0.5)/(1-0.05)^2*0.01/0.1=-0.045
- With those conservative assumptions, background only give about 5% error on signal asymmetry

Exclusive π+π−: missing mass dependence

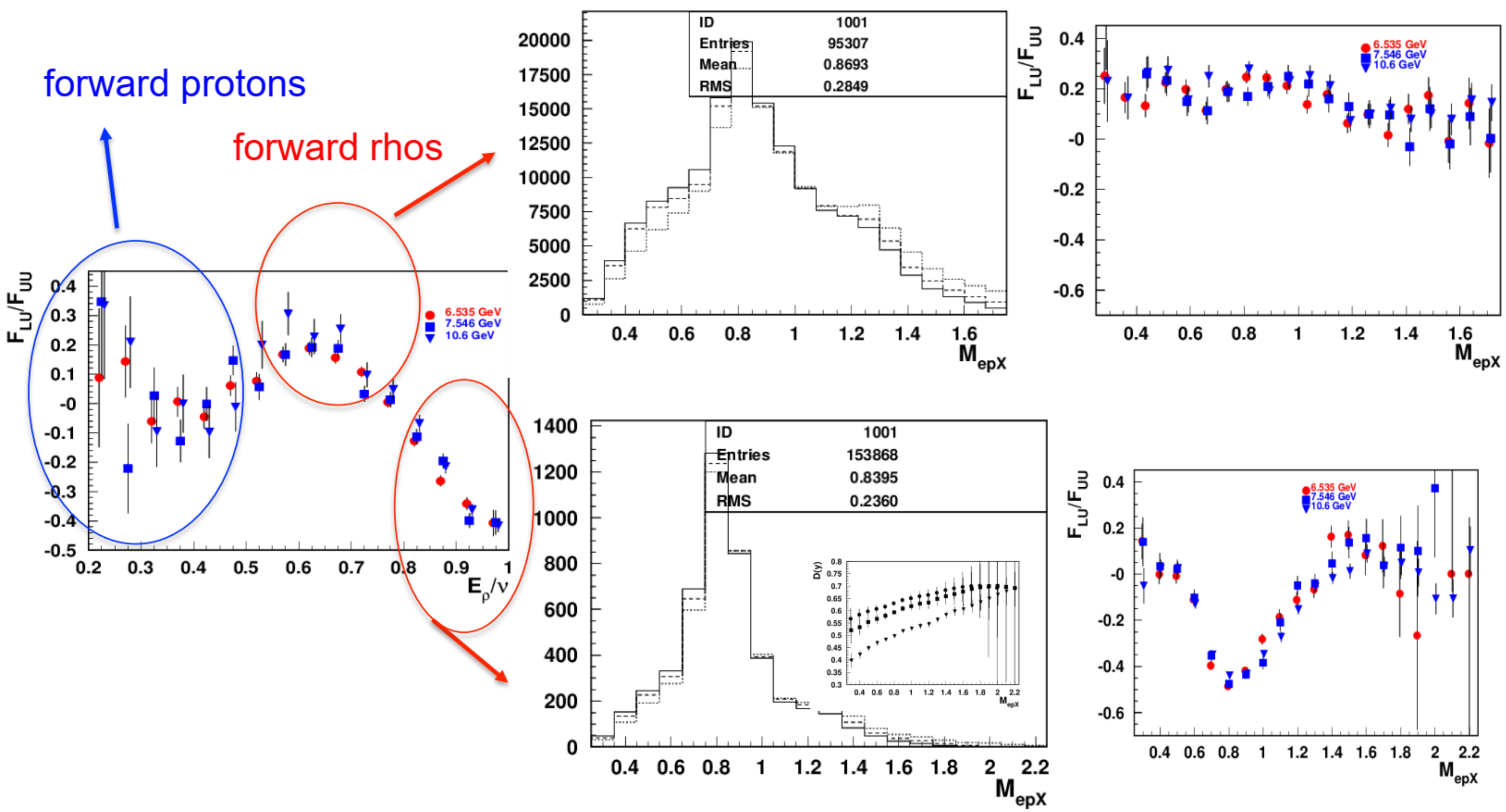

Rhos dominate both exclusive dihadron samples, contributing differently depending on z

Cost

System	Item	Cost (K$)
Tracker planes	uRWell	900
	VMM readout	300
	HV	10
	Mechanical	100
Scintillator planes	Scint. materials	640
	light guide	180
	PMT+base	180
	FADC	500
	HV	150
	Mechanical	100
Iron planes	Mechanical	200
Total		3,260

Table 1: Cost estimation of the forward angle muon detector and related hardware.

Binning

Bin	ξ' range	ξ range	t range (GeV^2)
1	$-0.255 < \xi' < 0$	$0.152 < \xi < 0.176$	$-5.541 < t < -0.287$
2			$-0.287 < t < -0.150$
3			$-0.150 < t < -0.020$
4		$0.176 < \xi < 0.739$	$-5.541 < t < -0.287$
5			$-0.287 < t < -0.150$
6			$-0.150 < t < -0.020$
7	$0 < \xi' < 0.512$	$0.071 < \xi < 0.126$	$-5.541 < t < -0.287$
8			$-0.287 < t < -0.150$
9			$-0.150 < t < -0.020$
10		$0.126 < \xi < 0.153$	$-5.541 < t < -0.287$
11			$-0.287 < t < -0.150$
12			$-0.150 < t < -0.020$
13		$0.153 < \xi < 0.189$	$-5.541 < t < -0.287$
14			$-0.287 < t < -0.150$
15			$-0.150 < t < -0.020$
16		$0.189 < \xi < 0.739$	$-5.541 < t < -0.287$
17			$-0.287 < t < -0.150$
18			$-0.150 < t < -0.020$
19	$-0.255 < \xi' < -0.017$	$0.071 < \xi < 0.108$	$-5.541 < t < -0.287$
20			$-0.287 < t < -0.150$
21			$-0.150 < t < -0.020$
22		$0.108 < \xi < 0.122$	$-5.541 < t < -0.287$
23			$-0.287 < t < -0.150$
24			$-0.150 < t < -0.020$
25	$-0.255 < \xi' < -0.040$	$0.122 < \xi < 0.152$	$-5.541 < t < -0.287$
26			$-0.287 < t < -0.150$
27			$-0.150 < t < -0.020$
28	$-0.040 < \xi' < -0.017$	$0.122 < \xi < 0.152$	$-5.541 < t < -0.287$
29			$-0.287 < t < -0.150$
30			$-0.150 < t < -0.020$

Table 2: Bin boundaries of the binning scheme shown in Fig. 24.

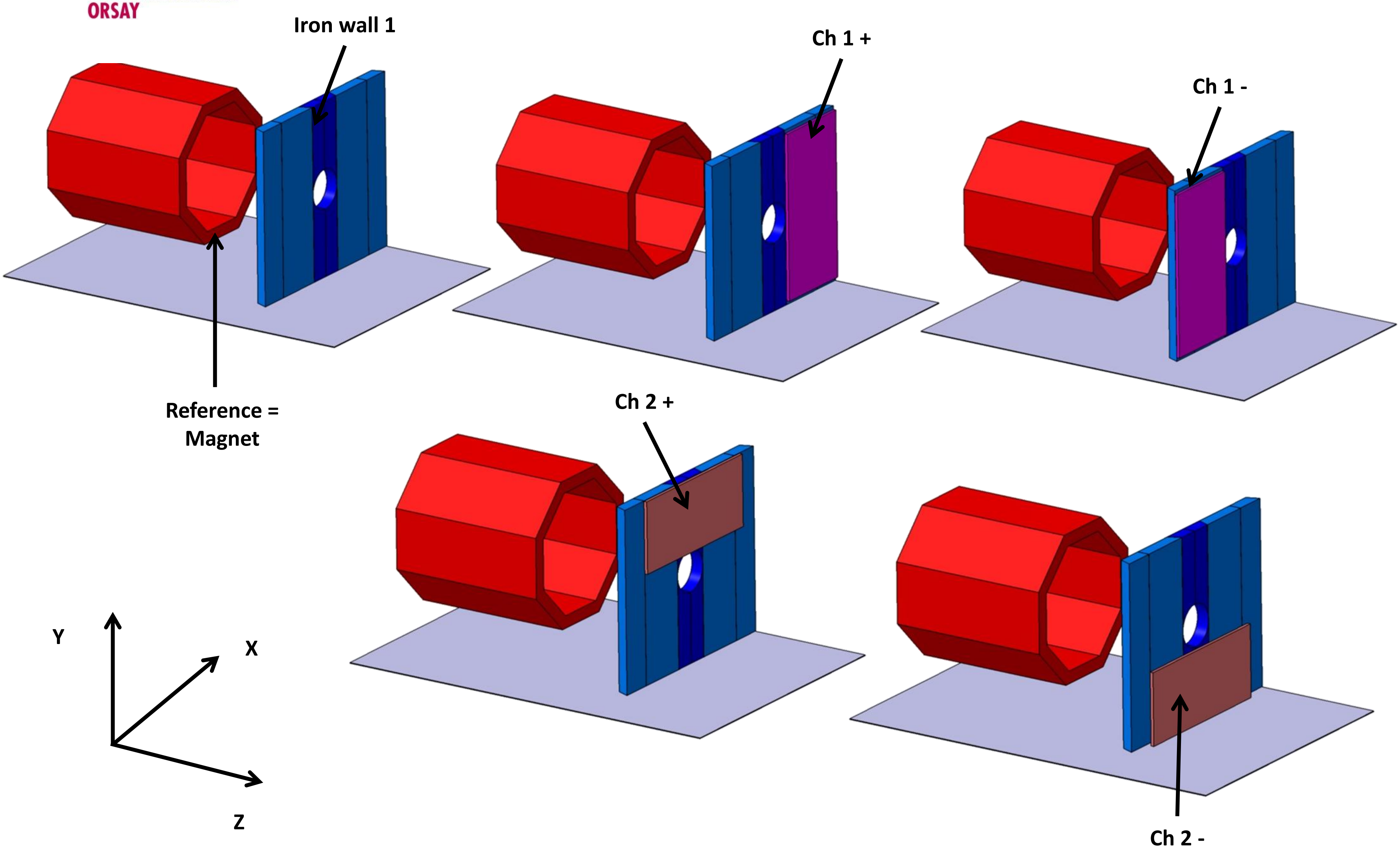
Iron wall 1
Ch 1 +
Ch 1 -
Reference =
Magnet
Ch 2 +
Y
X
Z
Ch 2 -

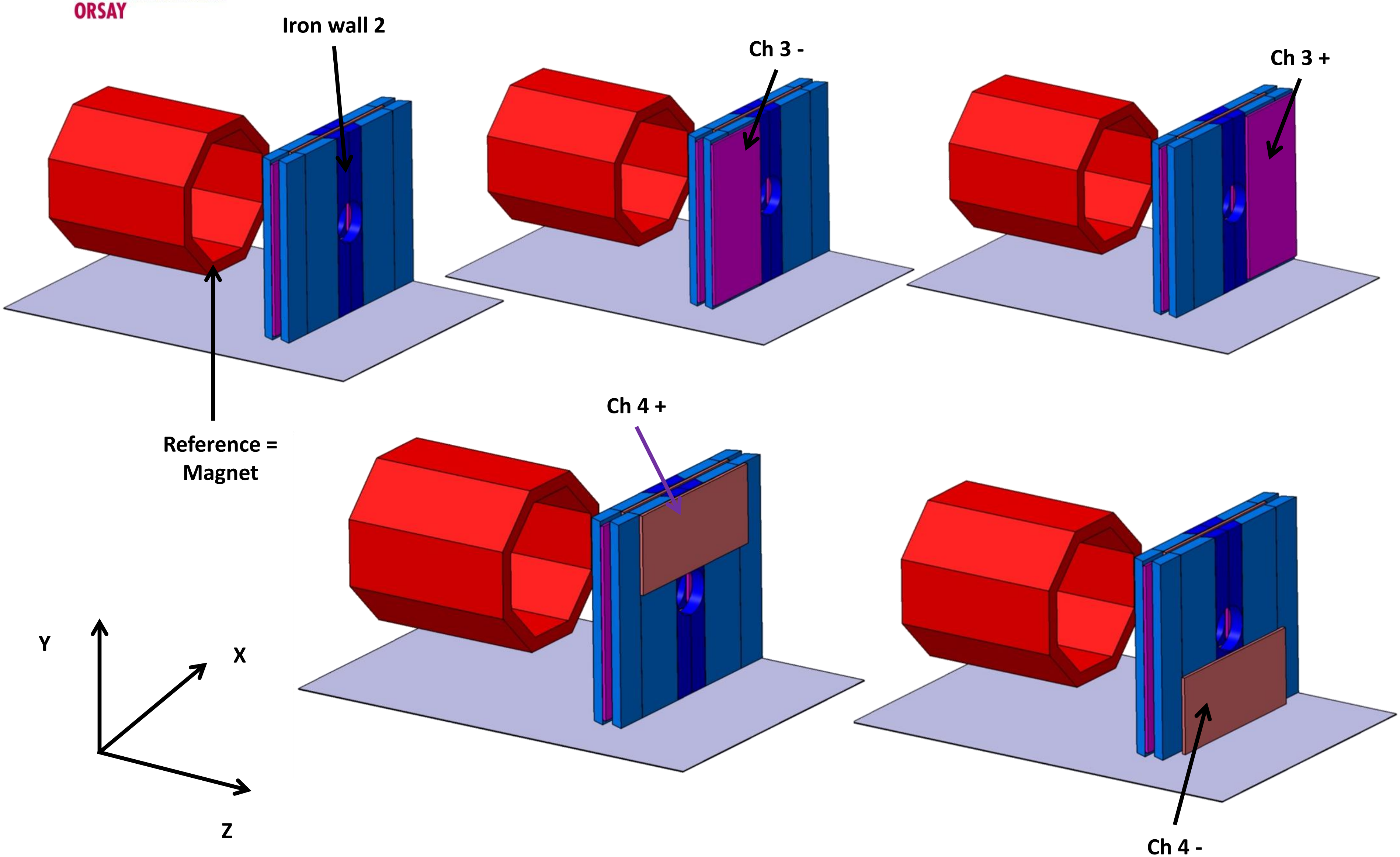
Iron wall 2
Ch 3 -
Ch 3 +
Reference =
Magnet
Ch 4 +
Ch 4 -
Y
X
Z

E12-12-006: Near Threshold J/Psi production on LH2 target

Most precise measurement near threshold

SOLID-J/Ψ PROJECTIONS

Precision at high t crucial for extrapolations to the forward limit (exponential, dipole, triple, …)

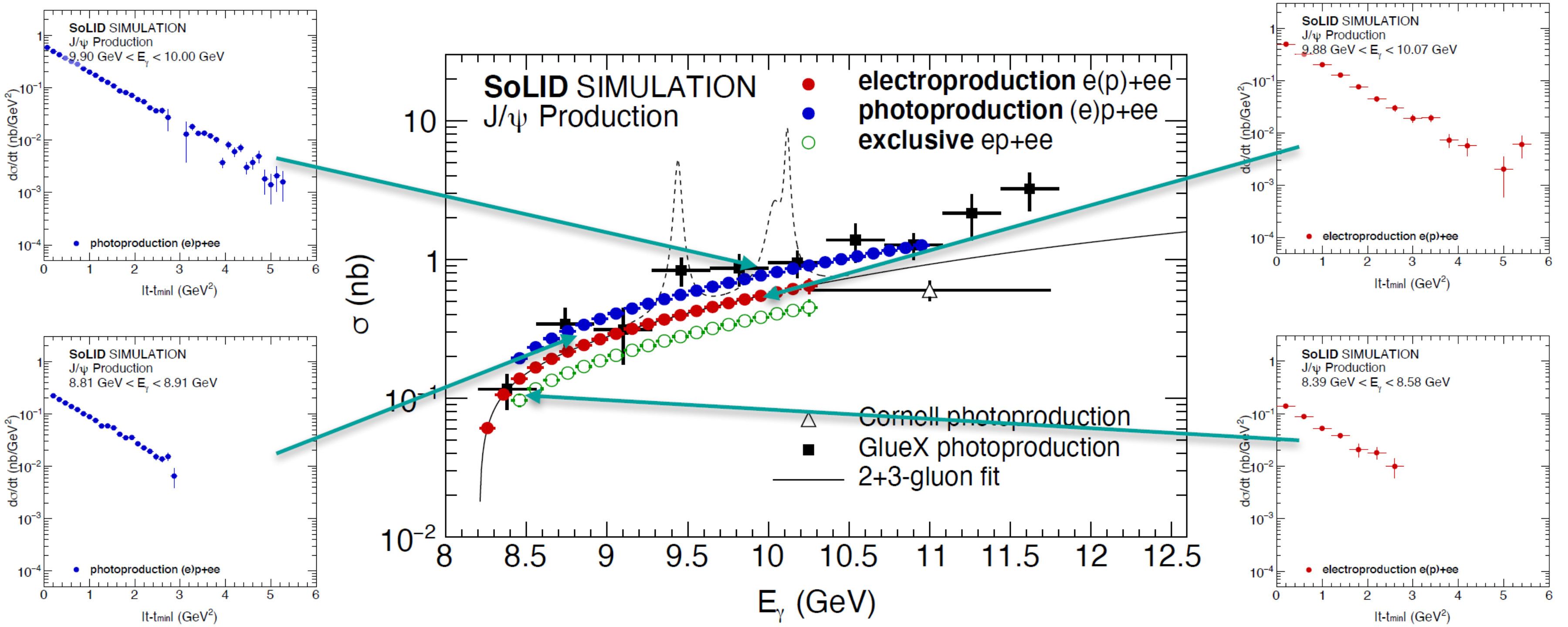

E12-12-006A: TCS with circular polarized beam and LH2 target

- SoLID TCS will have at least 1 order larger statistics than CLAS12 and usher TCS study into precision era with multi-dimensional binning
  - SoLID has 250 times more integrated luminosity than the CLAS12 TCS published result
  - SoLID acceptance to TCS events is about ¼ of CLAS12. But with full azimuthal coverage, (ideal for the forward backward asymmetry)
  - Crosssection measurement (moment)
- SoLID TCS could lead to study of NLO correction

SoLID TCS coverage

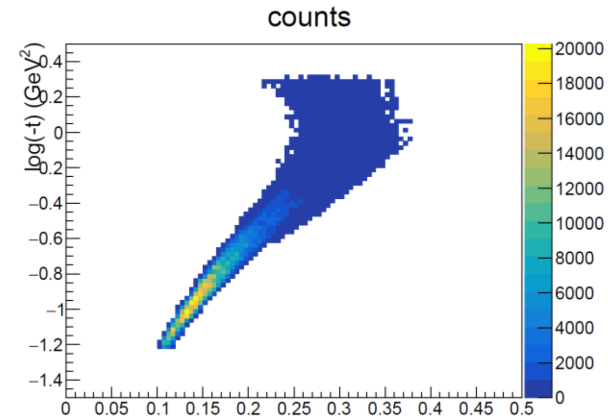

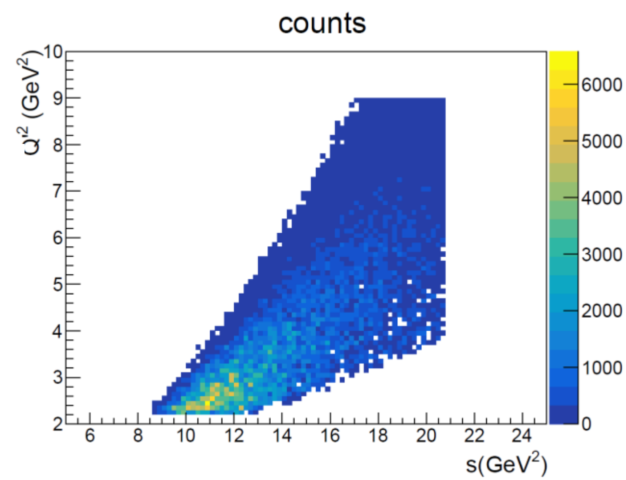

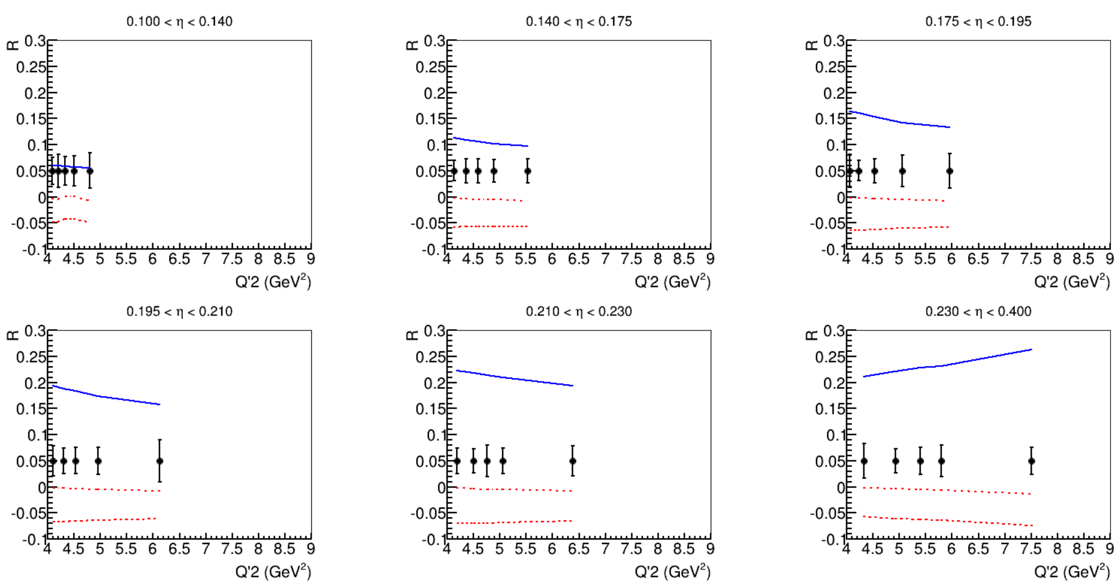

$$R = \frac{2\int_0^{2\pi} d\varphi \cos\varphi \frac{dS}{dQ'^2\, dt\, d\varphi}}{\int_0^{2\pi} d\varphi \frac{dS}{dQ'^2\, dt\, d\varphi}}$$

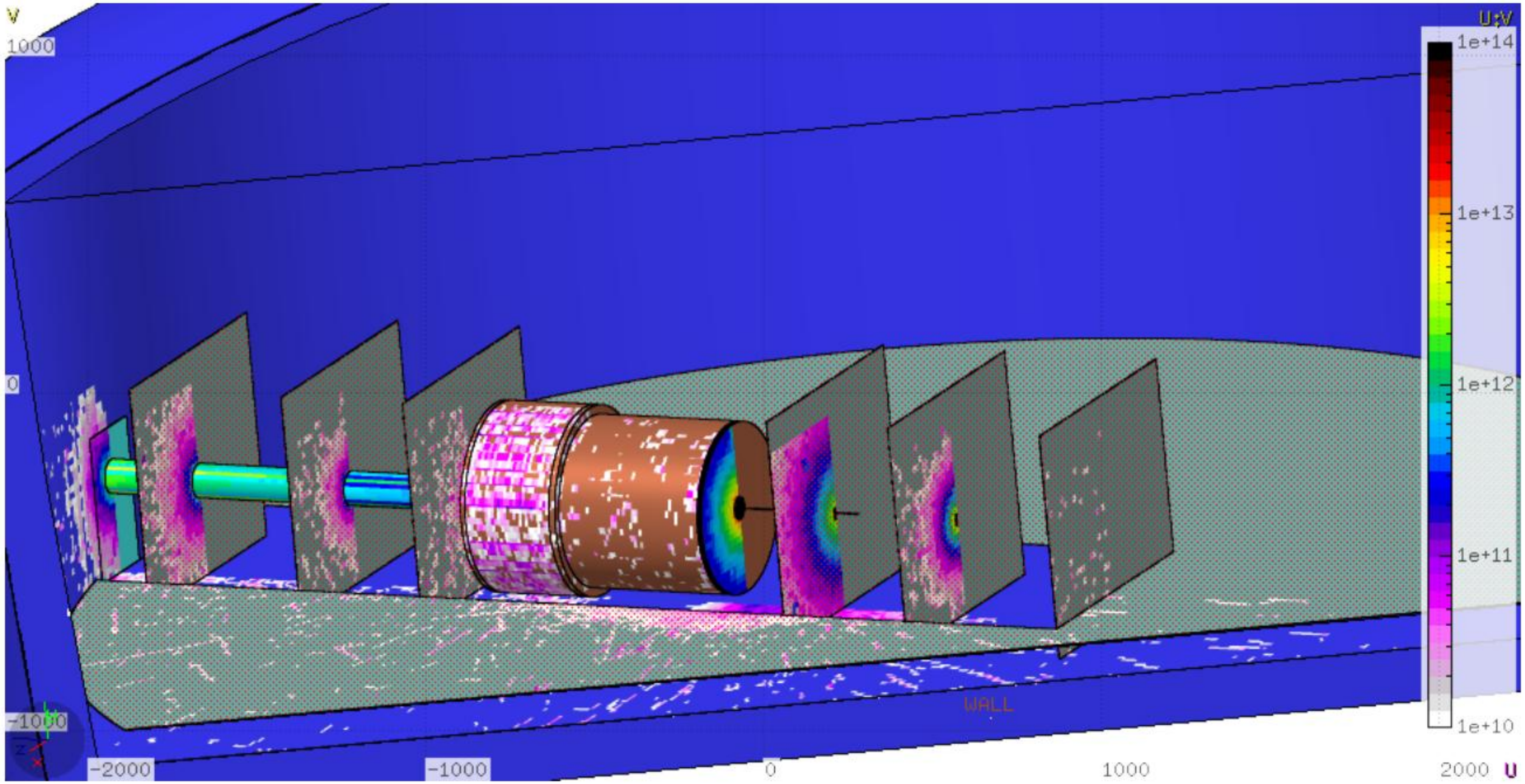

Figure 151: Estimate of radiation damage in the Hall with the SoLID spectrometer and the J/Ψ configuration with a 15cm Liquid Hydrogen target. The leading part of radiation present in the Hall for the SoLID spectrometer is originating from the target area and the closer surface of the magnet. In this plot, we show the 1MeV neutron equivalent flux per cm^2 on the volume surfaces estimated for 60 days of continuous running with a beam current of $3\mu A$ (This is the expected beam-time with the J/Ψ configuration). In order to better show the behavior of the radiation leaking, different planes of observation have been inserted (see Fig. 149a for reference of the position of each plane). The Color scale is different than in the previous cases in order to enhance the details in the desired region.